Phase Change Cooling for Low-Pressure Applications

Tim Aebersold

taebersold@student.ethz.ch
taebersold@swissloop.ch

Full-Scale Technical Research Submission
June 2023

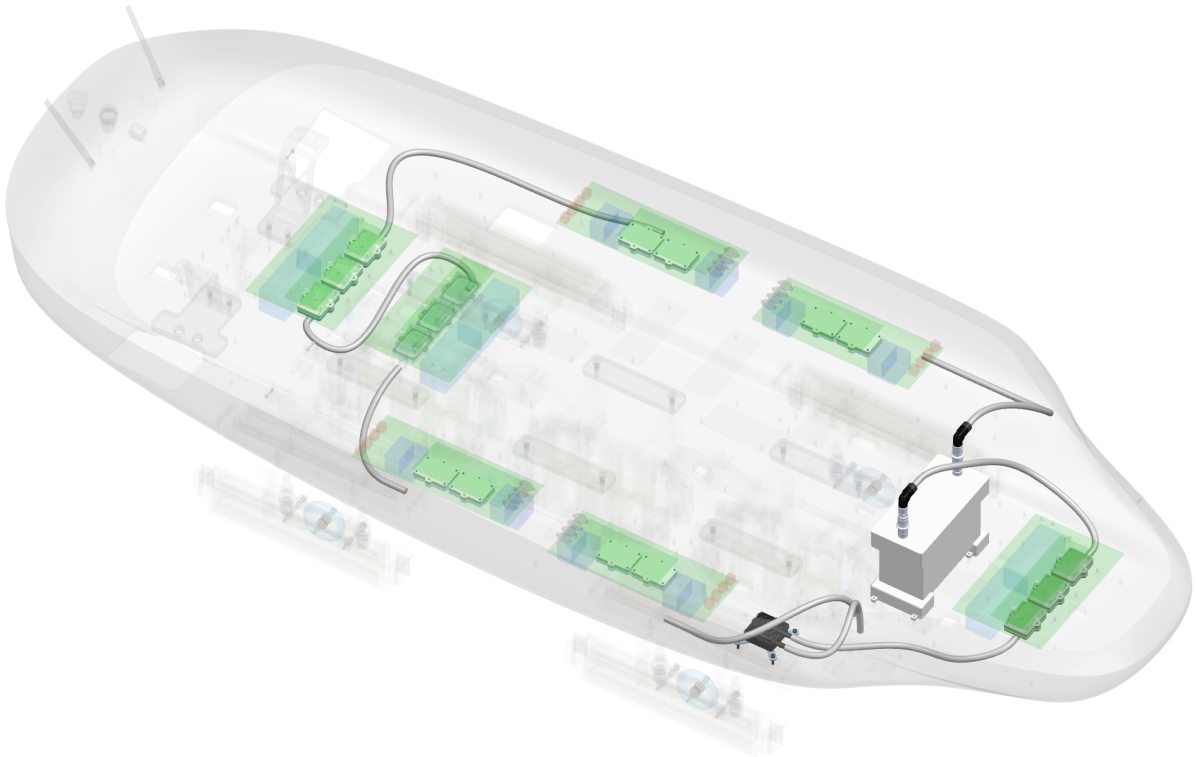

Dear Reader

This research submission is based on Tim Aebersold's bachelor's thesis "Design, Simulation and Manufacturing of a Phase Change Cooling Module for Low-Pressure Applications". In the thesis, the development of a phase-change thermal management system for the power electronics of this year's Swissloop pod, Bertrand Piccard, is described in detail. The aim of this thesis was to build a functional phase-change cooling module based on a concept suitable for full-scale Hyperloop operation. To be clear, the thesis is not meant contain a thorough full-scale feasibility study. Rather, it is mainly concerned with engineering specifics of phase-change cooling systems. This allows for critical (and sometimes unexpected) design considerations, such as the problems posed by thermal expansion during melting of phase change materials (PCMs), to be highlighted very early in the discussion surrounding phase change heat batteries.

With thermal management of Hyperloop systems operating at low tube pressures being a long-standing discussion point, we believe that phase change heat storage is one of the most promising approaches. Due to their favorable mass- and volume-specific heat capacity, PCMs make on-vehicle heat storage feasible. Other approaches are briefly delved into, as well.

This research submission is divided into two parts. In the first part, the thesis and its key takeaways are summarized concisely on a few pages **(Executive Summary)**, and further potential areas of interest are presented. In a second part, some selected sections of the original thesis are presented in detail, providing more in-depth information on some of the topics touched upon in the summary.

Best wishes,

Tim Aebersold
and the whole Swissloop Team

Part I

Executive Summary

To start, approaches to dissipate heat during operation of Hyperloop pods were investigated in Section 2.2.

Heat Dissipation

- Convection was found to not be sufficiently effective at low tube pressure of 10 mbar in 2.2.1.
- At higher tube pressures of roughly 100 mbar, the rough calculations provided here indicate that adequate heat dissipation can be achieved through convection if a large, heavy (> 500 kg), and drag-inducing radiator is used. (See 2.2.1)
- Radiation has been shown to be feasible in theory. Two methods of radiative cooling were presented in 2.2.2:
  - Using the pod's outer fairing for radiative dissipation. This requires very good in-plane heat conductivity in the fairing. Additionally, adequate insulation is needed to prevent heat back-flow into other parts of the vehicle (e.g. passenger cabin).
  - Alternatively, a radiative probe can be heated using on-board equipment as shown in Figure 2.3. Since $\dot{Q} \alpha T^4$, this vastly improves radiative heat transfer.

Heat Storage

- Instead of dissipating heat, it can be stored on the Hyperloop vehicle. The heat can then be rapidly retrieved while the vehicle is in standstill at its destination.
- Latent heat storage (heating of water, metals, or similar) is limited in its volumetric and weight-effectiveness.
- Combined structural-thermal usage of large vehicle components (e.g. the structural frame) is discussed in 2.3.3. While weight effective, this approach poses difficulty in rapid heat retrieval.
- Various types of phase-change (latent) heat storage were looked into:
  - Solid-solid phase change materials are good conductors and do not need special enclosures. However, their mass-specific enthalpy of phase change is limited as of now. (See 2.4.2)
  - Liquid-gaseous evaporation is extremely mass-effective. However, the expanded gas can not be feasibly contained within the vehicle as described in 2.4.1. The vapors would thus need to be vented into the low-pressure tube, causing secondary technical challenges for the tube owner.
  - Solid-liquid phase change materials have high volumetric and mass-specific (roughly 60 Wh/kg) enthalpy of phase change. They outperform sensible heat storage by a large margin.

Solid-Liquid Phase Change Materials

- It was found that heat transfer in solid-liquid phase change materials presents a key challenge due to limited thermal conductivity. A large portion (roughly 50%) of overall system mass is spent on the enclosure and heat transfer devices (fins) as previously assumed [1]. (See 2.4.3 and 5.2.1)
- Water was briefly considered as a PCM due to its high mass-specific enthalpy of phase change and excellent availability. It was discarded due to its low temperature of phase change T_{pc} of 0 °C at 1 bar, making it susceptible to melting while the vehicle is in idle.
- This poses a problem for small prototype vehicles running in open air during summer.
- In a full-scale environment for use in vacuum, a well-insulated water-based PCM module should be re-investigated.
- The suitable T_{pc} for a the built small-scale module was set to roughly 40 °C. T_{pc} should be low to improve heat transfer during melting, but high enough to prevent melting during outdoor use in summer.
- The two primary commercialized PCMs with suitable T_{pc} are salt hydrates and paraffin.
- Salt hydrate's advantages lie in volumetric energy density and thermal diffusivity (i.e. ease of heat transfer) as detailed in 2.4.3.
- Meanwhile, paraffin has slightly higher mass-specific enthalpy of phase change, is non-corrosive, and has less variability in cyclical stability. The thesis focuses on the engineering of a paraffin-based system for these reasons.

- It was found that paraffin's advantage in mass-specific enthalpy of phase change is offset by the mass saved in heat transfer devices (fins) and enclosure mass if salt hydrates are used. This is due to their thermal diffusivity and high density. Thus, overall, salt hydrates make for lighter and more compact PCM heat storage units than paraffin-based systems.
- Improving thermal conductivity with additives as described in 2.4.4 was found in 5.2.1 to reduce the need for fins, lowering system mass.
- PCMs were extensively modelled in COMSOL. The enthalpy of phase change was accounted for through a modified heat capacity method as described in 3.4.
- Here, the PCMs were modelled as liquids with large viscosity in their solid state and continuous transition during melting. This allowed for simulation of natural convection in PCMs.
- It is generally assumed that natural convection slightly improves heat transfer. The use of additives impedes natural convection due to increased viscosity. No further studies have been conducted regarding this trade-off.
- Taking natural convection into account vastly increases solving times of models.

The thesis then goes into the some engineering specifics of PCM cooling systems.

Architecture

- Decentralized architecture: Phase-change cooling units are spread out over the vehicle, close to the heat sources. Heat is retrieved by flushing coolant through a loop connecting these units. (See 3.2.1)
- Centralized architecture: PCM is located in a single, large container. Heat transfer from sources to liquid is realized through dedicated coolant loops or similar (e.g. conduction with heat pipes). Heat retrieval can occur either by flushing, or by physically replacing ("swapping") the centralized module. (See 3.2.2).
- For the prototype system built, a centralized architecture was chosen. Manually swapping the module is an advantage during testing. A centralized module is also more flexibly usable, since components with unusual shapes (e.g. hollow copper wires in coils) can be cooled.
- Here, the heat transfer from sources to PCM module was implemented with water.
- Using liquid PCM as a heat transfer medium was briefly considered, but is complex to engineer due to the high viscosity of the PCM (requires special pumping equipment) and risk of solidification in the coolant lines.
- As of currently, fins (or other fin-like arrays) are seen as indispensable for adequate heat transfer, making the use of PCMs as heat transfer media superfluous.
- Figure 5.1 shows how a centralized PCM module could be combined with electrical energy storage, and swapped rapidly during stops at destinations.
- If longer stops at destinations are tolerable, flushing with coolant is feasible. This would allow for a decentralized architecture, which could be advantageous from packaging and weight standpoints.

Stuctural Integrity and Thermal Expansion

- It was found that paraffin and salt hydrate PCMs undergo drastic expansion during melting (roughly 5% to 15%).
- When opting for a fully enclosed PCM system, this causes excessive internal pressures.
- In a full-scale system, a system of pressure relief valves is needed to avoid the resulting stresses on the enclosure.
- For the small-scale prototype system, it was found that such valves would introduce unwanted complexity and weight. The 2023 Swissloop pod phase change module's PCM chamber is fully sealed.
- To deal with the expansion from melting, a large airgap was used to reduce the rise in pressure as described in 3.6.1.
- The 2023 small-scale PCM module is highly mass-optimized and was produced using Selective Laser Sintering (SLS) of aluminium.

Further Areas of Interest

Some of the subjects which could be investigated in further detail include:

- Extended feasibility study of a PCM cooling system for full-scale Hyperloop based on well-founded power consumption estimates.
- Prototyping of a system employing a heat pump to warm up a small radiation probe for small- or full-scale systems.
- Drag and convective heat dissipation of a fin array at 50 - 100 mbar needs to be investigated using CFD methods.
- Study on optimal additive ratios and the use of salt hydrates. Explore the mass and volume effect on overall PCM cooling systems. (Trade-off between the thermal conductivity and capacity of PCMs).
- Tackle the drawbacks of salt hydrates (corrosion, cyclical stability, manufacturer reputation and availability). If these can be addressed, salt hydrates are an attractive alternative to paraffin, since they make for lighter and more compact systems.
- Design of an autonomous system for rapid quick-swapping of PCM modules.
- Design of a pressure relief system for full-scale operation.
- Examine thermal management of Li-Ion battery cells using PCMs. The battery as a heat source has been entirely neglected for the purposes of the original thesis, but will be relevant in full-scale use.

Part II

Shortened Thesis: “Design, Simulation and Manufacturing of a Phase Change Cooling Module for Low-Pressure Applications”

Acknowledgements

I would like to acknowledge and thank the following organizations for their contributions to this project: Feramic (Stallikon) for producing the prototype cooling module body and lid, Schindler (Ebikon) for milling the waterblocks, Eloxalwerk Züri-Oberland (Wetzikon) for anodizing the waterblocks, Maagtechnic (Dübendorf) for providing material for the gaskets, Stäubli (Horgen) for providing the fluid quick-connectors at a discount, Prodartis (Appenzell) and Verticalprint (Winterthur) for help with the waterblock lid, and Swissloop (Dübendorf) for providing some financial assistance with the project.

I would also like to thank Simon Maranda and Sebastian Ammann from HSLU (Luzern) for advice with modelling of PCMs and practical advice on handling PCMs, Richard Leblois from Elinter (Cham) for extensive discussions surrounding modelling and design, Carsten Flake of EPSE at ETH Zurich for help with SLA printing, Patrik Postweiler at RWTH (Aachen) for initial discussion of system-wide modelling, Ivan Šuta and Umberto Romito from Museum für Gestaltung (Zürich) for photographing the components, Anna Bürgi for proof-reading, Basil Gross and Luca Rufer for their help with testing, and the whole Swissloop team for providing inputs for the prototype cooling system and helping with integration into the vehicle.

Special thanks goes to Jan Seiler, my supervisor from EPSE at ETH Zurich, for his guidance and support throughout the project.

Abstract

Thermal management in Hyperloop systems is a significant challenge due to low pressure environments which impede convective heat transfer. This thesis explores suitable concepts for thermal management, with a focus on latent heat storage using PCMs.

A fully functional PCM cooling system with a weight of 6.5 kg and peak power capacity of 1750 W (400 W continuous) was designed and manufactured. The system is designed for a small-scale Hyperloop test vehicle for use in student competitions. It employs a paraffin PCM in a selective laser sintered (SLS) enclosure. Simulations were used to optimize and characterize the system's performance. The system was comissioned successfully. The potential of alternative approaches for thermal management, including water tanks, radiation and convection was also discussed.

Contents

List of Acronyms

CF	Carbon Fiber
CFD	Computational Fluid Dynamics
CFRP	Carbon Fiber Reinforced Polymer
CNC	Computerized Numerical Control
EDS	Electrodynamic Suspension
EG	Expanded Graphite
EMS	Electromagnetic Suspension
EPDM	Ethylene Propylene Diene Monomer
FDM	Fused Deposition Modelling
FEM	Finite Element Method
FJM	Fusion Jet Modelling
HEMS	Hybrid Electromagnetic Suspension
IPU	Inverter Power Unit
LIM	Linear Induction Motor
LPU	Levitation Power Unit
LSRM	Linear Switched Reluctance Motor
MOSFET	Metal-Oxide Semiconductor Field-Effect Transistor
NBR	Nitrile Butadiene Rubber
PCB	Printed Circuit Board
PCM	Phase Change Material
SLA	Stereolithography
SLS	Selective Laser Sintering
VCU	Vehicle Control Unit

Introduction

In the development of Hyperloop systems, the challenge of cooling electronics in a near-vacuum environment is still unsolved. This submission is based on the thesis "Design, Simulation and Manufacturing of a Phase Change Cooling Module for Low-Pressure Applications", which documents in great detail the development of a small-scale prototype thermal management system for the 2022/23 Swissloop pod.

To start, a brief overview of possible cooling concepts (convection, radiation, latent heat storage) is provided. Then, phase change cooling is examined in detail in this thesis. First, the potential of phase change cooling on a full-scale system is analyzed. Second, the simulation, design and manufacturing (along with some limited testing) of a small latent heat storage prototype is discussed in detail in Chapter 3. The built small-scale system can be used by Swissloop in prototype vehicles over the coming years. As a third step, the practical learnings can be used to formulate some recommendations for a large-scale phase-change cooling system (see Chapter 5).

Concept

To begin, the conditions a full-scale vehicle would encounter are explained in detail.

2.1 Problem Setting

The envisioned vehicle will travel in a low-pressure environment of between 5 and 100 mbar [2]. Therefore, natural convection as a means of cooling is severely limited. With various on-board heat sources ranging from motors and power electronics to air conditioning, thermal management presents a key issue for the Hyperloop concept. In the following sections, the feasibility of various means of thermal management are discussed. First, a focus is put onto dissipation using convection and radiation. As a second step, various means of heat storage, like sensible and latent heat sinks, are discussed. For the sake of this thesis, a full-scale vehicle with the following dimensions was used as a benchmark for various cooling solutions:

- Vehicle length: 10 m
- Vehicle height and width: 2.5 m
- Trip duration: 60 min (equivalent to Zurich - Rome or Zurich - Hamburg)
- Time between trips: < 10 min

On-board heat generation between 4 kW and 8 kW is assumed. Of this, 1 kW of heat generation is allocated for air conditioning for 10 passengers. 3 kW of heat is allocated for the levitation, and 4 kW for propulsion losses. Depending on the route, the propulsion is not always active. These figures are loosely based on Swissloop's experience with building prototypes. However, the dimensions, passenger capacity and power consumption of a full-scale vehicle could differ drastically from these figures.

For the small-scale prototype vehicle built by Swissloop in 2022/2023, the heat loss is 440 W for 15 minutes. Detailed boundary conditions (dimensions, power figures) for the small-scale prototype are discussed in detail in Section 3.1.

Goals

The goals of a cooling system with full-scale feasibility are three-fold. First, the electronics and passengers need to be kept sufficiently cool during high-speed travel runs. Second, this cooling must be repeatable. The vehicle should be able to do multiple runs a day without overheating, i.e. a sustainable form of heat management is necessary. Third, the time between runs should not be dictated by thermals. Here, it was prescribed that the time in between trips should not exceed 10 minutes.

2.2 Dissipation: Convection and Radiation

To achieve sustainable dissipative thermal management, a quasi-stationary state of heat transfer from the vehicle to its surroundings needs to be achieved. The three principal methods of stationary heat transfer are conduction, convection and radiation. Since the vehicles are envisioned to fully levitate, they will not touch any of their surroundings. As such, heat conduction was excluded from the outset. Below, convection and radiation are examined in more detail.

2.2.1 Convection

Dissipating heat through convection could be achieved as shown in Figure 2.1. Low-pressure air is channeled through a large array of fins, which in turn cools on-board electronics.

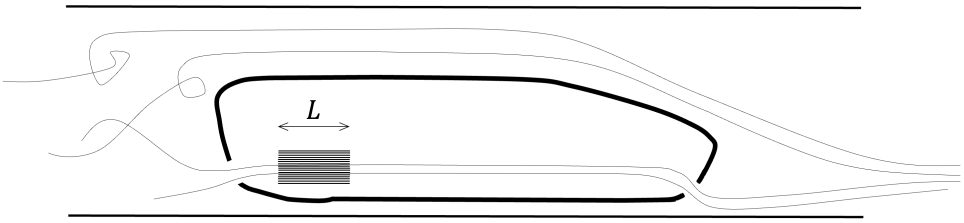

Figure 2.1: Low-pressure Convective Cooling. Using a fin array significantly increases the area available for heat transfer.

Theory: Gas Regime

To apply adequate correlations describing convective heat transfer, the flow regime the sparse air in the tube falls under must first be determined. The Knudsen number indicates the flow regime low-pressure gases abide by [3], as shown in Table 2.1.

Table 2.1: Flow Regimes of Gases. The Knudsen number expresses the importance of individual molecules on gas behaviour. The correlations describing convection vary drastically over these regimes.

		Kn	<	0.001	Continuum Regime
0.001	<	Kn	<	0.01	Slip Flow Regime
0.1	<	Kn	<	10	Transition Regime
10	<	Kn			Molecular Regime

In the continuum regime, inter-molecular effects are relevant, and a fluid can be treated as a continuum. In this regime, fluids behave as is typical for gases around atmospheric conditions. Typical models for approximating convective heat transfer can be used [4]. On the other end of the spectrum, for example if pressure is low or the gas is confined to a small physical system, lies the molecular regime. Here, the behaviour of a gas is dictated by single molecules. For example, heat conduction between a vehicle and tube wall for $K_n > 10$ would not occur through a series of particle collisions in a continuous gas. Rather, individual particles would transfer heat by travelling between two walls directly, avoiding collision with other particles. In this regime, convective heat transfer models valid at atmospheric conditions fail.

The Knudsen number is defined as [4]:

$$Kn = l/L \tag{2.1}$$

where l is a molecules free mean path, and L is a system's characteristic length. The free mean path l for a gas is given by [5]:

$$l = \frac{k_B T}{\sqrt{2}\pi d^2 p} \tag{2.2}$$

Table 2.2: Material Values and Key Figures Used for Estimation of Convective Heat Transfer.

	10 mbar	100 mbar
μ	$1.81 \cdot 10^{-5}$ Pa s	$1.81 \cdot 10^{-5}$ Pa s
ρ	0.0119 kg/m^3	0.119 kg/m^3
λ [7]	0.008 W/mK	0.022 W/mK
c_p	1.003 J/kgK	1.003 J/kgK
Re_L	$0.73 \cdot 10^5$	$7.3 \cdot 10^5$
Pr	2.26	0.822
$\overline{Nu}$	39.3	6.00
$\overline{\alpha}$	0.0959 W/m^2K	0.264 W/m^2K
$\dot{Q}$	2.1 kW	5.8 kW

where k_B is the Boltzmann constant, T is the temperature and p the pressure of the gas, and d the molecular diameter. To find the range of Kn for the specific problem at hand, T is set to 293.15 K. Furthermore, it is assumed that p is between 10 and 100 mbar, and that d for air is 4 Å. In the envisioned tube environment, the free mean path of air as formulated in Equation 2.2 would thus be between 647.8 nm and 6478 nm. To get an approximation of Kn, the characteristic system length L has to be set. Here $L = 0.5m$ is chosen, since this will be the length of the flow over the fin array.

Using Equation 2.1, Kn is calculated to be between $1.3 \cdot 10^{-5}$ and $1.3 \cdot 10^{-6}$. Therefore, the air in the shown system lies firmly within the continuum regime. All further computations for the convective heat transfer can thus be made using similar methods as used at atmospheric conditions.

Theory: Convection on Fins

While convective skin cooling on the outer fairing could be possible, an array of cooling fins fed through an air inlet is used as a basis for computations here. A central fin array can be placed physically close to heat sources, reducing issues with integration and heat transfer. It is assumed that the fin array (similar to an automotive radiator) is 2 m in width, 1 m in length, and 0.5 m in height at most to fit into the vehicle. The fin array consists of 100 stacked metal sheets of 1 mm thickness each, making for a surface area A of 400 m^2. Perfect heat conduction is assumed in the metal. The convective flow is assessed as a laminar flow over a planar surface according to [6].

The density shown in Table 2.2 is calculated from the ideal gas law at 293.15 K. The dynamic viscosity μ of air is assumed to be exclusively dependent on temperature. Shown below are the material properties used in the following calculations. First, the occurrence of turbulence was examined. The Reynolds number at the flow exit ($L = 0.5m$) is given by:

$$Re_L = \rho \cdot \frac{u_\infty L}{\mu} \tag{2.3}$$

where u_∞ is the incoming flow velocity of 222 m/s (800 kph). Since $Re_L > 10^5$ for the 100 mbar case, the flow is expected to be turbulent. For the case of 10 mbar tube pressure, the flow is laminar. Next, the Prantl number is dependent on heat capacity c_p, thermal conductivity λ, and dynamic viscosity μ.

$$Pr = \frac{c_p \mu}{\lambda} \tag{2.4}$$

The results for both Prantl and Reynolds number are both noted in Table 2.2.

Theory: Turbulent Convection

For the turbulent case (100 mbar of tube pressure), the local Nusselt number is given by:

$$Nu_x = 0.0296 \cdot Re_x^{4/5} \cdot Pr^{1/3} \tag{2.5}$$

with Re_x being the local Reynolds number. Derived from this, the average Nusselt number over the fin length can be found using [6]:

$$\overline{Nu} = 0.0296 \cdot Pr^{1/3} \cdot (\frac{u_\infty \rho}{\mu})^{4/5} \cdot \int_0^L x^{4/5} dx \tag{2.6}$$

.

From $\overline{Nu}$, the length-averaged heat transfer coefficient $\overline{\alpha}$ can be found [6]:

$$\overline{\alpha} = \overline{Nu} \cdot \frac{\lambda}{L} \tag{2.7}$$

and, finally, from $\overline{\alpha}$ the possible heat flow from convection:

$$\dot{Q} = A \cdot \overline{\alpha} \cdot \Delta T \tag{2.8}$$

with ΔT being the temperature between metal fins and the gas in the tube. Here, the gas temperature is set to 20 °C. Furthermore, it is assumed that for efficient operation the temperatures of on-board electronics are not allowed to exceed 80 °C during steady state operation. Due to some small thermal resistances, it is assumed that the fins have a temperature of 75 °C. ΔT is thus 55 °C.

The expected heat flow from convection at 100 mbar ($\overline{Nu}$ = 6) using equations 2.3 to 2.8 is 5.8 kW. Relevant intermediary values are noted in Table 2.2. This means that, for the higher end of feasible tube pressures, convection can be a sufficient means of heat dissipation. There is, however, significant drag associated with the use of a large fin array. Additionally, it would be heavy at a mass of 540 kg for the aluminium sheets exclusively, not yet factoring in additional hardware. Lastly, for lower pressures the heat transfer significantly decreases, as shown in the following section.

Theory: Laminar Convection

Since $Re_L < 10^5$, a different correlation for Nu_x is used here [6] and rewritten to a similar form as Equation 2.6:

$$\overline{Nu} = 0.332 \cdot Pr^{1/3} \cdot \sqrt{\frac{u_\infty \rho}{\mu}} \cdot \int_0^L x^{1/2} dx \tag{2.9}$$

In the laminar case at 10 mbar, the power which can be dissipated using a fin array is only 2.1 kW. Again, intermediary steps are note in Table 2.2. This decrease from 100 mbar is caused by following effects:

- Due to the flow being laminar, heat transfer to the fluid decreases.
- The incoming air has low density and thus low heat capacity.
- Thermal conductivity is significantly lower.

All of these effects trace back to the low pressure.

Conclusion

At higher pressures, where propulsion concepts based on air turbines is being conducted [8], convective heat transfer can be sufficient. While 5.8 kW of dissipation is in the desired range, extensive research has to be put into optimizing the ratio of heat transfer to drag of a large fin array.

At 10 mbar, the dissipative performance relative to weight, drag and space usage is underwhelming. With this, convection is ruled out as a suitable means of heat dissipation at lower pressures approaching 10 mbar. For all further investigation, focus is put on this low pressure (10 mbar) scenario.

2.2.2 Radiation

Radiative heat transfer depends on the geometries and materials used in vehicle and tube. Still, a simple model is used to assess radiation. Ideal values are assumed wherever possible to determine an upper limit of cooling through radiation.

Theory: Cylinder Approximation

To this end, the vehicle geometry is approximated as a cylinder as shown in Figure 2.2. The radiative heat transfer between an inner and outer hollow cylinder is given by [9]:

$$\dot{Q} = \frac{A_1 \sigma (T_1^4 - T_2^4)}{\frac{1}{\varepsilon_1} + (\frac{A_1}{A_2}) \cdot (\frac{1}{\varepsilon_2} - 1)} \tag{2.10}$$

where subscript $_1$ represents the inner cylinder (vehicle) and subscript $_2$ the outer cylinder (tube). The area A relates to model depth and circumference, meaning the flat ends of cylinders are not involved here.

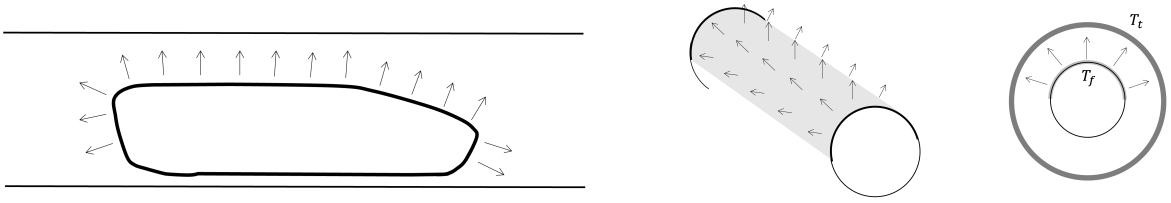

Figure 2.2: Left: Radiative Dissipation on Outer Fairing. Right: Substitute Model. The substitute model represents the pod as a cylinder.

The Stefan-Boltzmann constant is given as:

$$\sigma = 5.67 \cdot 10^{-8} \frac{W}{m^2 K^4} \tag{2.11}$$

The pod emmisivity ε_1 and tube emissivity ε_2 are assumed to be equal to 1. The area of the vehicles outer fairing A_f replaces A_1, rendering the following equation:

$$\dot{Q} = A_f \sigma (T_f^4 - T_t^4) \tag{2.12}$$

with T_f being the temperature of the vehicle fairing and T_t being the temperature of the tube. Conservatively, T_t is set to 40 °C to represent outside air on a European summer day.

Furthermore, as before it is assumed that the maximum allowed electronics temperature is 80 °C. Due to thermal resistances between electronics and fairing, these electronics are likely to be significantly warmer than the outer fairing. Thus, it is assumed that the outer fairing can be held at a maximum of 65 °C. With a vehicle length and diameter of 10 m and 2.5 m respectively, and assuming that roughly 50 % of the surface area can be used for radiation, a radiative heat transfer of 7.7 kW can be reached.

It must be noted, however, that elevated outer fairing temperatures raise some issues. First, the vehicle must be well-insulated from the hot outer fairing. Otherwise, inadvertent back-flow of heat into sensitive components and passenger cabin can occur. Second, sufficient in-plane heat conductivity is necessary in the fairing. Otherwise, the fairing's in-plane thermal resistance can easily act as a bottleneck. In this case, a given needed heat flow is associated with large temperature gradients over the fairing, leading to excess temperatures at the heat sources. Enabling in-plane heat flow poses a significant engineering challenge, especially with weight and aerodynamics as competing goals.

On the other hand, $\dot{Q} \, \alpha \, T_f^4 - T_t^4$ is a quartic relationship of heat flow and temperature. Therefore, slightly raising fairing temperatures by decreasing thermal resistance vastly enhances radiative heat dissipation. For example, bringing T_f from 65 °C to 70 °C increases $\dot{Q}$ by 23 %.

This leads to another possible method of radiative heat transfer. Using a heat pump, a probe can be heated to very high temperatures. By thermally insulating it from the vehicle, it can dissipate heat with very small surface area. The concept is shown in Figure 2.3.

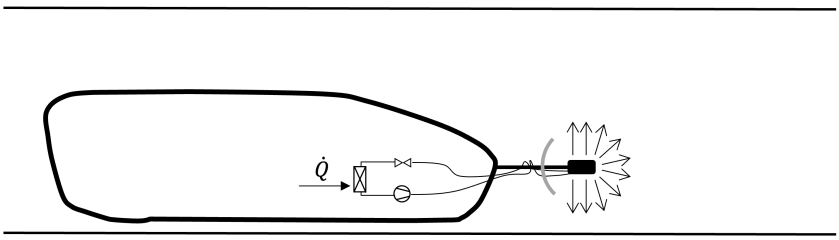

Figure 2.3: Radiative Dissipation with Heat Pump and Probe. Using the heat pump, high temperatures in the probe can be achieved, which drastically increases radiative heat transfer.

Conclusion

In this example, with 7.7 kW being firmly in the 4 kW - 8 kW range, enough cooling can be provided. With radiative heat transfer being independent from air as the heat transfer medium, the cooling performance is independent of tube pressure. Thus, to conclude, it can be stated that radiation has clear potential as a cornerstone of thermal management in Hyperloop vehicles. However, only a brief assessment has been conducted with two possible approaches stated. Further research is thus needed.

Furthermore, it is impossible to test radiation in everyday usage on small-scale prototypes during summer outside of a tube. The high amount of radiative heat input from the sun would render a radiative cooling system unusable. Thus, it is much harder to discover operational flaws of a prototype system, so that the idea was not pursued any further. Following below, focus is shifted from dissipation of heat to another promising form of thermal management: storage. Through discharging rapidly between runs, storage can become operationally sustainable. First, sensible heat storage is looked at.

2.3 Sensible Heat Storage

Sensible heat storage occurs when a material's temperature raises as it is supplied with heat. Generally it holds:

$$\dot{Q} = c_p \cdot m \cdot \Delta T \tag{2.13}$$

In the past, sensible heat storage has been used by Swissloop on prototype vehicles. Aluminium, due its low cost, high c_p and λ, makes for a suitable heat sink for short, high-power applications.

2.3.1 Aluminium Heat Sink and Other Metals

However, for usage in longer timeframes, sensible heat storage is not suitable due to its low thermal capacity. The maximum allowed ΔT is set to 40 °C. Using Equation 2.13 with aluminium (888 J/kgK), and integrating over time, one obtains:

$$m = \frac{t \cdot \dot{Q}}{\Delta T c_p} \tag{2.14}$$

At 8 kW over a time t of one hour, the mass for an alumnium heat sink is equal to 810 kg. At 440 W over 15 minutes (Swissloop Prototype), this figure is reduced to 11.15 kg. For reference, the latent heat storage module shown later needs less than 1.4 kg of PCM to reach a similar capacity. There are no metals with higher heat capacity than aluminium known to the author. With this, metals are discarded as a primary heat storage device for the given application.

Gases were previously discarded as sensible heat storage materials due to volumetric constraints in the envisioned usage scenario. Among solids, there are few materials (ceramics, polymers, ...) with higher specific heat capacity than aluminum. When it comes to fluids, however, some perform very well.

2.3.2 Water

Water, and some fluids used with it in automotive and rail applications, such as alcohols (e.g. glycol), have a very high specific heat capacity. At 440 W for 15 minutes with ΔT = 40 °C, 2.36 kg of water would provide the needed thermal capacity. (172 kg at 8 kW for 60 min.) Water is easy to handle, can be run directly through heat exchangers, and is cheap. Considering this, it seems like a suited heat storage medium for the given application. However, water is still 40 % heavier than PCM with equivalent capacity at $\Delta T = 40$°C. If the tolerable ΔT were smaller, PCMs would outperform water by an even larger margin.

2.3.3 Combined Structural and Thermal Usage

Other than using water, another potential way of improving the mass-specific capacity of sensible heat storage is simultaneous structural and thermal usage of components. With Aluminum (888 J/kgK) and carbon fiber reinforced plastics (CFRP, 1040 J/kgK) making up a large fraction of structural materials in mobility applications, there is a high likelihood that the needed thermal mass on a high-speed vehicle would already be present in structural components. Figure 2.4 shows a component as typically used in Swissloop vehicles. This component is optimized for structural loads. With few adaptations, however, it could serve as a heatsink.

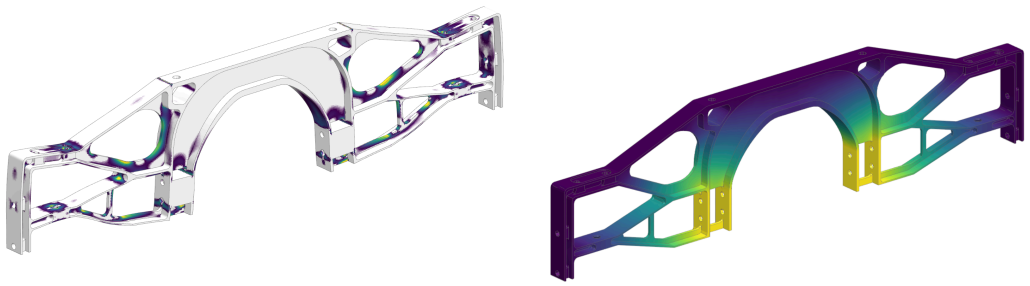

Figure 2.4: Structural Vehicle Component Used as Heatsink. Left: Stresses, Right: Temperatures. Simultaneous structural and thermal usage allows for weight savings.

Both CFRP and aluminium do not experience a loss in structural performance in the temperature range between 0 °C and 80 °C. Therefore, if thermal expansion can be accounted for, a ΔT of 40 °C can easily be tolerated by structural components used as heatsinks. Some hardware might be needed to ensure heat transfer from electronics into structural parts. However, the capacity weighs virtually nothing since no material needs to be added for capacity. Like water, this seems an ideal solution at first glance.

Heat Transfer and Entropy

However, there are some issues with such a solution:

1. Structural considerations can lead to geometries not optimal for heat transfer (e.g. thin walls). Optimizing for both criteria is not trivial.
2. Large structural components spanning a whole vehicle might generally less suited for good heat transfer. The path of heat flow can be long, increasing temperature gradients.
3. With the warming of structural components, heat leakage into other parts of the vehicle tends to increase. Thus, for combined thermal-structural usage, a relevant amount of heat will be released into unwanted areas (e.g. passenger cabin). A more centralized metal heatsink or water tank would perform better in this regard, but might still require significant amounts of insulation.
4. The problem of large-scale diffusion of heat and leakage into other components also increases the difficulty of rapid heat retrieval during vehicle stops.

2.3.4 Conclusion: Use as Complementary Storage

It has been shown that sensible heat storage such as water or metal heat sinks can be lacking in terms of mass-specific thermal capacity despite large ΔT. Still, these solutions come with some benefits:

1. Water, and other fluids, can be pumped. Thus, retrieving warmed water from a vehicle tank is rather simple. As such, water is very suitable for rapid retrieval between consecutive vehicle runs.
2. Both water and aluminium make for great heat transfer media. Water, through its ability to be pumped, can be heated very homogeneously at a heat source. The result is good heat transfer and in consequence low electronics temperatures. Similarly, aluminium has a high thermal conductivity. Thus, both are well-suited for applications with relatively large bursts in heat.

The second point makes these materials a great choice as intermittent heat sinks. They can be used to dampen power peaks during usage, and as heat transfer media. Both water and aluminium are extensively used in the small-scale prototype described later. To achieve greater mass-specific capacity, the solution proposed below is using phase change materials.

2.4 Phase Change (Latent Heat Storage)

Three modes of phase change were considered: Liquid-gaseous phase change, solid-solid phase change, and solid-liquid phase change.

2.4.1 Liquid-Gaseous Phase Change

Of these three, liquid-gaseous phase change (evaporation) can by far achieve the highest mass-specific enthalpy of phase change. For evaporation, the temperature of phase change is highly dependent on pressure. This allows for a tunable temperature of phase change by adjusting the pressure a liquid/vapor mixture is under.

Table 2.3 shows various options that were considered for use as phase change media. At a pressure of 1 bar, various alcohols have a suitable temperature of phase change. These include methyl acetate and methyl iodide, chloroform, acetone, carbon disulfite and many more. As an alternative approach, gases can be kept at high pressures (e.g. ammonia) or at low pressures (e.g. water) to achieve the desired phase change temperature. However, for all of these options, the volumetric expansion inherent to liquid-gaseous phase change poses severe issues. First, keeping constant pressures at changing volumes in an isolated system is challenging and requires heavy and space-consuming parts, like pumps or bladders. Second, as seen in Table 2.3, liquid-solid phase change is volumetrically inefficient.

To illustrate this point, the volumes of a solid-liquid and liquid-gaseous PCM on the Swissloop prototype are computed. At roughly 300 kJ of storage capacity, 1.5kg of solid-liquid PCM with 200 kJ/kg is required. When evaporating water at 80 mbar with an enthalpy of phase change equal to 2403 kJ/kg, the density of the fully evaporated water is 18.1 m^3/kg [10]. The resulting volume is roughly 2.3 m^3. For a small prototype vehicle of 2.5 m x 1 m x 1 m, the phase change thermal management unit would thus consume almost all of the available space in the vehicle. In a full-scale application, the large volume fraction of a passenger cabin makes space concerns more relevant. Thus, the volume occupied by a liquid-vapor PCM is seen as even less feasible in these scenarios. While some pressurized gases, like ammonia, perform slightly better, their volume-specific capacity is still lacking. All together, a liquid-gaseous phase change in a closed system was ruled out.

Table 2.3: Volume Usage and Mass-Specific Capacity of Liquid-Gaseous PCMs. The large volumes occupied by the gaseous PCMs (v_{vap}) make them volumetrically ineffective compared to a solid-liquid PCM like paraffin.

	h_{pc}	Pressure	T_{vap}	v_{vap}
Carbon Disulfite [11]	355 kJ/kg	1 bar	46 °C	$\sim$0.35 m^3/kg
Methyl Acetate [12]	405 kJ/kg	1 bar	57 °C	$\sim$0.35 m^3/kg
Ammonia [10]	1094 kJ/kg	16 bar	41 °C	0.09 m^3/kg
Water Vapor [10]	2393 kJ/kg	0.1 bar	47 °C	14.67 m^3/kg
Paraffin RT 43 HC	240 kJ/kg	1 bar	43 °C	0.0013 m^3/kg

As an alternative to a closed system, the evaporated gases can be vented into the vacuum tube during operation. From a vehicle-centric perspective, this represents an ideal solution. However, this approach comes with extensive measures which have to be taken to retrieve these vapors from the tube environment over large volumes. For sustainable operation, the evaporated liquids need to be retrieved using specialized pumps. Hence, the option of liquid-gaseous phase change is discarded.

2.4.2 Solid-Solid Phase Change

Solid-solid phase change materials are not as widely commercialized as liquid-solid PCMs. There are, however, some advantages to these "solid state" PCMs [13]:

- Small volume change during phase change
- No need for encapsulation

For the few commercially available solid-solid PCMs, the mass-specific capacity was found to be significantly lower than for salt- or paraffin-based PCMs. Typical enthalpies of phase change for solid-solid PCMs are roughly 100 kJ/kg [14], compared to double that for solid-liquid PCMs. Additionally, density and thermal conductivity are both in similar ranges as paraffin and salt hydrate PCMs. While ongoing research does not exclude future usage of solid-solid PCMs, it was concluded that the drawbacks of commercially available solutions outweighed the advantages. Therefore, these were discarded as well.

2.4.3 Solid-Liquid Phase Change

With solid-solid and liquid-gaseous phase changes discussed, a third available option is employing solid-liquid phase change materials.

Water/Ice

One option for a solid-liquid PCM is water, i.e. the melting of ice. This phase change comes with a very high enthalpy of phase change at 333 kJ/kg. Since this phase change occurs at 0 °C, operating a latent heat storage unit would pose issues of unwanted melting. In particular, during usage on the Swissloop prototype at atmospheric pressure during summer, melting will occur at significant rates even when the vehicle is not in use. To combat this, significant amounts of insulation are needed to prolong the duration of passive melting. Similarly, in a full-scale vehicle in vacuum some leakage inevitably occurs, for example from a heated passenger cabin.

For a prototype vehicle, this means that using a water-based PCM cooling system is associated with impractical handling concerns. For example, the vehicle can not be left sitting for too long between test runs, which is a major inconvenience during testing. Water as a phase change material was thus discarded for the system being built here.

In a full-scale prototype, water could be investigated further, as it does come with some advantages. Melted water is easy to pump, and also has a high sensible heat capacity c_p. For such an application, the amounts of insulation needed would have to be examined in more detail to determine full-scale feasibility.

Hydrated Salts

Salt hydrates pose one alternative to water. Typically, a crystalline solid of the form AB·xH2O is formed from inorganic salts (AB) and water [15]. Here, the "melting" occurs through dehydration of the salt. Salt hydrates usually melt to a salt hydrate with fewer moles of water, or to its anhydrous form. During this transition, liquid water released from the hydrated salt dissolves the formed nonhydrated salt molecules [15]. For commercially available salt hydrate PCMs, the maximal operating temperatures are limited to roughly 20-30 °C above melting temperature [16, 17].

Salt hydrates are affordable and widely available. They are, for example, commonly used in hand warmers. However, salt hydrates can lack cyclical stability. Depending on manufacturing quality and composition, the performance of hydrated salt PCMs can decrease drastically over time according to talks with industry experts.

A large disadvantage of hydrated salt PCMs is that, depending on composition, they can be corrosive to metals. A circumstance which, if metal heatspreaders are planned to be used, requires additional engineering to prevent long-term corrosion. Hydrated salts come with improved density over water and other solid-liquid PCMs, and are thus preferable in volume-critical applications. However, the mass-specific enthalpy of phase change is lower than with other PCMs, which can be a drawback. Table 2.4 compares the key performance characteristic of a typical hydrated salt PCM with a paraffin alternative.

Paraffin

Paraffin (from latin "parum affinis", little reactivity) typically consists of multiple aklane types with the form C_nH_{2n+2}. For paraffins, the hydrocarbon chain length expressed by n influences the melting temperature and enthalpy of phase change. Generally, more pure compositions limit the temperature of phase change to narrow temperature range.

Parrafin is a by-product of the petro-chemical industry and is commonly used in candles, vasoline, and similar everyday products. Due to well-established, large-scale manufacturing processes, paraffin in higher grades is affordable and can be purchased from a variety of vendors. As a PCM, paraffin is available at a wide range of phase change temperatures and possesses high specific enthalpies of phase change. Additionally, it shows high cyclical stability, meaning melting and subsequent solidifaction can be repeated over a long lifespan [18]. Generally, more consistent quality is expected from paraffin PCMs across manufacturers and their product ranges. This is not the case with salt hydrates.

Both paraffin and hydrated salt PCMs suffer from low thermal conductivities [19]. In many applications, the resulting temperature gradients in the PCM can cause insufficient cooling at the heat source. Thus, measures have to be taken to ensure adequate heat transfer. Very commonly, the PCM is placed in a metal enclosure with fins.

Table 2.4: Typical Hydrated Salt and Paraffin PCMs.

	RT 35 HC [18]	SP 31 [16]
T_m	35 °C	31 °C
h_{pc}	210 kJ/kg	180 kJ/kg
λ, k	0.2 W/mK	0.5 W/mK
ρ_s	0.88 kg/L	1.35 kg/L
	Inert	Corrosive

While paraffin achieves slightly higher mass-specific capacity (Table 2.4), hydrated salts are both denser and have significantly higher thermal conductivity. In effect, higher density also contributes to elevated heat capacity, since the path length heat has to travel is reduced. This can be summarized by thermal diffusivity α, given as:

$$\alpha = \frac{k}{\rho \cdot c_p} \tag{2.15}$$

, with PCMs with larger α possessing improved heat transfer characteristics. Due to their lower α, it is likely that hydrated salt PCMs require less heatspreader material than paraffin-based PCMs at a given heat flow. Thus, despite lower mass-specific capacity, the overall system is likely to be lighter than with paraffin. Figure 2.5 shows this idea graphically. The paraffin heatspreader is significantly larger and thus heavier, offsetting the weight advantage of paraffin.

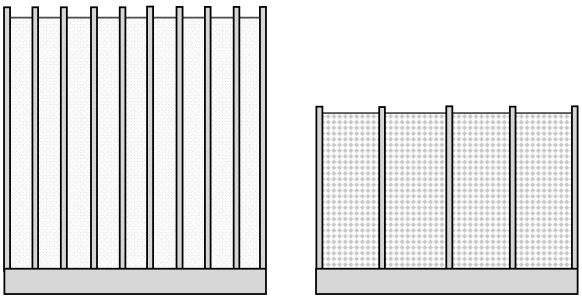

Figure 2.5: Size Comparison of Heatspreader for Paraffin and Salt Hydrate PCM. Left: Paraffin-based PCM with heatspreader. Right: Salt hydrate PCM with heatspreader. The density and thermal conductivity of salt hydrates allow for a smaller heatspreader with fewer fins.

Despite the volume and weight advantages of salt hydrates, the decision was ultimately made to employ a paraffin PCM here. Two major factors played into this choice. First, to avoid corrosion of the PCM container, the chemically inert paraffin is advantageous. Second, the reliability concerns for salt hydrates meant that only one manufacturer (Rubitherm Technologies, Berlin) was taken into consideration for this PCM type. However, their limited product range meant that no salt hydrate with a suitable temperature of phase change could be found.

2.4.4 Improvement of Thermal Conductivity

With paraffin as the PCM of choice, a significant issue is limiting the mass of metal needed for an adequate heatspreader at given heat transfer goals. To this end, additives such as alumina powder, expanded graphite or short-strand carbon fiber are commonly used in PCMs.

Existing Research

There is extensive research on this topic. A few relevant insights are highlighted here, with focus on additives used for hydrated salt and paraffin PCMs.

Fukai et al. [20] experimented with carbon fibers of lengths 5 mm to 200 mm in paraffin and hydrated salts. They found that careful orienting of the fibers can enhance thermal conductivity, and characterized the relationship between carbon fiber volume fraction and composite thermal conductivity. To give an example, they found that 2 % carbon fiber can increase the thermal conductivity of paraffin six-fold to 1.2 W/mK.

Karaipekli et al. [21] compared carbon fiber and expanded graphite additives in stearic acid. They found that expanded graphite (and to a lesser degree carbon fiber) does not separate from the PCM during repeated melting. Despite expectations that these additives would settle due to their higher density, they were cyclically stable.

Similarly, Frusteri et al. [19] demonstrated a stable suspension for short-strand carbon fibers in a hydrated salt PCM. Analogously to paraffin and fatty acid based PCMs, correlations between volume fraction of additives and thermal conductivity could be found. Frusteri et al. also note that homogeneous distribution of additives in the PCM affects results.

Using extensive computational fluid dynamics (CFD) studies, Shatikian et al. [22] studied the effect of metal fin dimensions on the melting of paraffin PCM. These studies account for natural convection

caused by buoyancy of melted paraffin, which has lower density than in solid state. The modelling of melting and convection of PCMs is discussed in detail below.

Overall, extensive research on the topic has been conducted. For bothm paraffin materials used, RT 35 HC and RT 44 HC, the manufacturer (Rubitherm Technologies, Berlin) claims compatibility with graphite additives. These additives, however, cause increased viscosity and potentially impede the fill-in procedure of the PCM. Employing additives in the prototype cooling module was briefly considered, but later discarded due to time constraints. For future versions of the prototype PCM cooling module or in full-scale applications, employing additives should be considered.

Design for Prototype

This chapter details the design of a complete PCM-based cooling system. It is significantly shortened. However, the original thesis [23] is supplied along with this research submission, providing full detail.

Built with the small-scale Swissloop prototype of 2022/2023 in mind, the system will see use until summer 2023 with use at the European Hyperloop Week. At the time of writing the thesis (January 2023), the real-world performance of the system could not be assessed yet.

3.1 Boundary Conditions

Heat Source: Battery

The 2023 Swissloop pod has a Lithium-Polymer battery (800 V, 250 A). It is assumed that in full-scale applications, the battery is a heat source which requires cooling. In the future, in particular for long operations in vacuum, this subject certainly needs to be tackled. However, it has been decided to not cool the battery on the prototype. Ordering a custom battery that would allow for tab cooling would have exceeded the production time frame, making it impossible to build a working battery system in a year. It has also been found that on the prototype, during the default mode, the battery mass can easily absorb the heat generated through internal resistance.

Heat Source: Electromagnets

The second major heat sources are the electromagnets in the motor and levitation system. Like with the battery, it is evident that eventually these electromagnetic actuators must be actively cooled for continuous use at near-vacuum. Thus, implementing active cooling of the levitation system was initially considered as a proof of concept. Specifically, removing heat by using water as a heat transfer medium was looked at. This could be achieved by using hollow copper windings [24] or incorporating polymer tubing into the windings. As an alternative, the steel core could be fitted with internal water channels, or an external heatspreader could have been pressed onto the windings.

Brief transient simulation using FloEFD and adiabatic wire temperature calculations lead to the conclusion that the electromagnetic systems did not require any active cooling in the 2023 Swissloop project year, so that it was left out for simplicity.

Heat Source: Power Electronics

Shown in Figure 3.1 are the Inverter PCBs used by Swissloop. On the power electronics for propulsion ("Inverter") and for levitation ("LPU"), the MOSFETs used for switching current present the centerpiece of the power eletronics. Active cooling of these MOSFETs is indispensable. As alluded to, past years have seen sensible heat storage (aluminium heat sinks) and air cooling as practical solutions. The LPU and Inverter MOSFETs have different footprints, but use identical mounting hardware. Thus, it was possible use a single heatsink design for both.

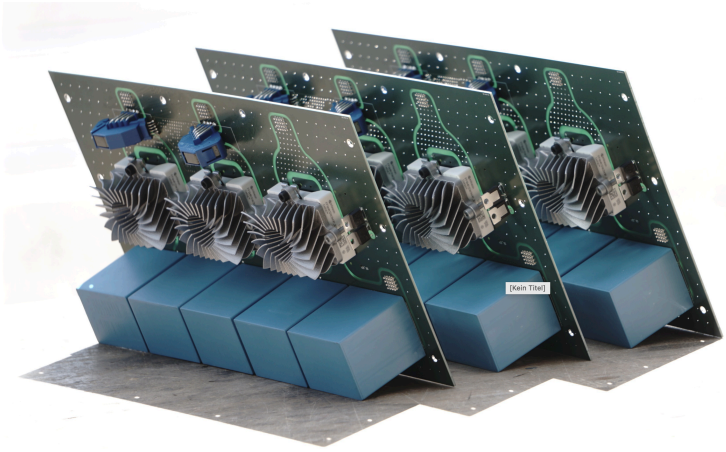

Figure 3.1: 2021/2022 Inverter Power Boards with Air Cooling [25].

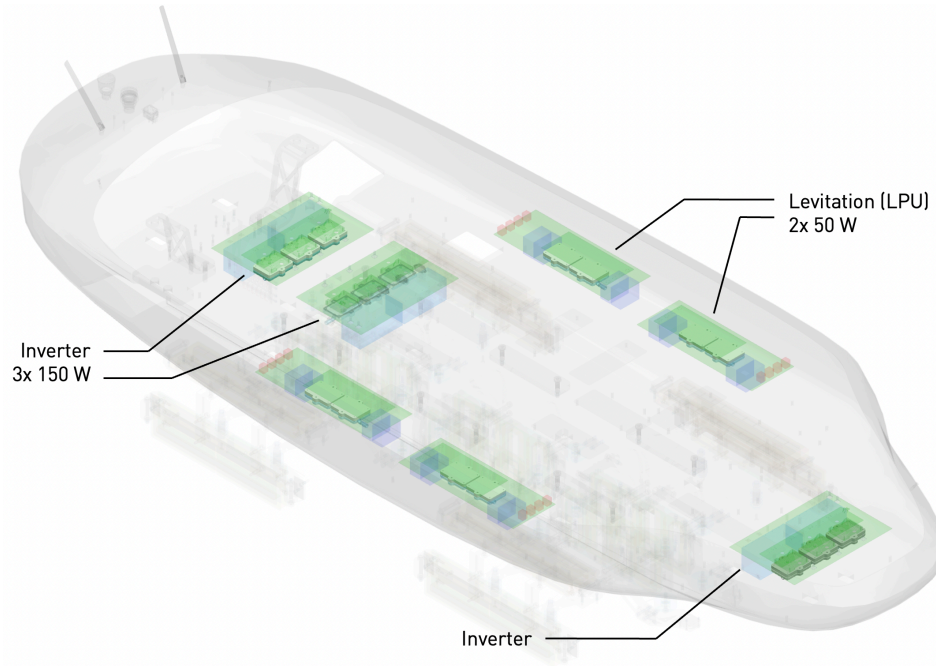

Figure 3.2: Heat Sources on 2022/2023 Swissloop Vehicle.

An overview of the heat sources is provided in Figure 3.2.

System Requirements

To summarize, the cooling system is built around the following power profiles:

- Handle multiple 10 s bursts of 9x 150 W and 8x 50 W (track run mode).
- Dissipate 8x 50 W over 15 minutes (standstill levitation mode).

Here, the standstill levitation mode dictates the needed energy capacity of the PCM for the cooling system. At four boards with two MOSFETs each, a total number of eight MOSFETs produce 400 W over 15 minutes. Conservatively, this figure was assumed to be 440 W. This exceeds the overall energy dissipated by 15 normal track runs (10 s each) occuring in a single day.

In addition to these power figures, the following requirements were set early on for the cooling system:

- The complete cooling system should not exceed a weight of 7 kg, since pod acceleration and levitation are highly sensitive to vehicle mass.
- Temperatures of up to 35 °C in summer should not impede the functionality of the cooling system.
- The power boards are mounted with the MOSFETs facing downwards. Thus, they are not easily accessible. The cooling system can not rely on easy accessibility of the MOSFETs.
- Built for vacuum: Structural integrity, in particular for use in levitation mode at near-vacuum needs to be guaranteed.
- Safety hazards for other pod components and human operators should be considered and minimized.

3.2 System Architecture

A major decision early on in the design process was the fundamental system architecture. Roughly, it was known how much PCM was needed to absorb the produced heat. However, two options were identified as to the distribution of that PCM: Decentralized or centralized. Figure 3.3 shows these two approaches. In the figure, a water loop is shown in dark blue. The patterned material represents a PCM, and grey represents metal.

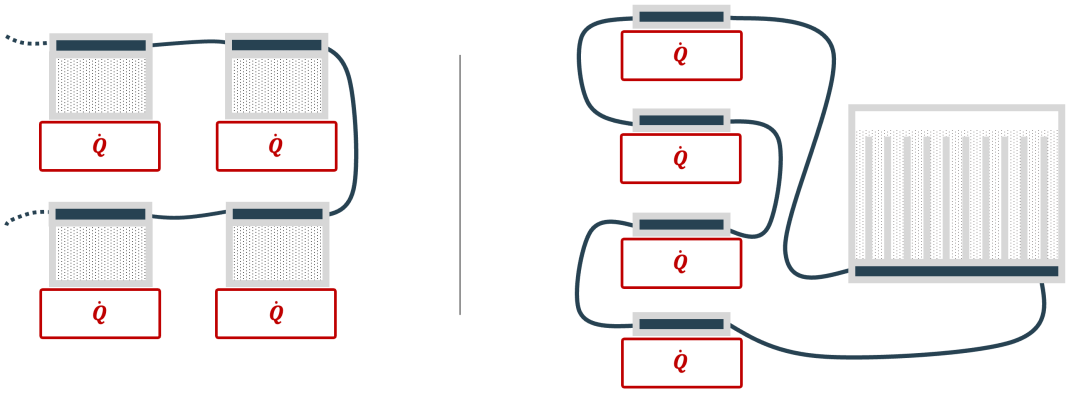

Figure 3.3: Left: Decentralized Architecture. Right: Centralized Architecture. During operation, the decentralized architecture employs the water loop for heat transfer.

3.2.1 Decentralized Architecture

The decentralized architecture approach centers around placing PCM as physically close to the heat sources as possible. The major advantage of this approach is good heat transfer, as the thermal path from source to PCM is short. Since these decentralized parts are not well accessible, tubing connects them. In-between runs, they can be flushed with coolant from an external pump. With the pump not on the vehicle, some weight is saved.

There are, however, multiple disadvantages. First, space restrictions on the PCBs might make it impossible to fit enough PCM into a decentralized container. All of these require tubing ports, with water chambers for flushing, a PCM chamber, and potentially heat spreaders. These add up to considerable volume for each decentralized PCM container. The second, more restricting downside, relates to design flexibility. Using the decentralized approach, the designed solution can only ever be used for power electronics. If, for example, the electromagnets need to be cooled, a completely separate new design is needed.

3.2.2 Centralized Architecture

With regards to flexibility, a centralized architecture is hugely advantageous. Once the PCM container (here: module) is built, it can be used for various purposes. Generally, it is assumed that designing

a fluid heat spreader at a heat source requires less specific knowledge than designing a PCM module. Thus, a centralized module can be used in future vehicles, with only adaptations to the fluid circuit. In the development cycle at Swissloop, this flexibility is highly valuable for coming vehicle designs. It allows for the centralized module to be used in future prototypes without a complete redesign, independent of MOSFET type and electromagnet dimensions. Thus, the centralized architecture was chosen here.

As an additional benefit, the centralized approach allows for more efficient usage of the available PCM material. During the standart track run mode, for example, the Inverter MOSFETs produce a majority of the dissipated energy. Meanwhile, in the levitation mode, the LPU MOSFETs produce the majority of dissipated energy. In the decentralized approach, the needed PCM capacity on these MOSFETs is not fully used. The centralized approach allows for full usage of capacity independent of use case, reducing the needed amount of PCM.

A disadvantage of the centralized approach is inferior heat transfer. As a partial solution to this issue, the fluid loop and metal heat spreaders on the MOSFETs are used as intermediary buffers.

For removing heat after runs, two options were considered. The first consists of flushing with the fluid loop. This necessitates an external reservoir of cold fluid and operation of the pump during vehicle standstill. Alternatively, and considerably simpler in usage, is module swapping. Here, two centralized modules can be swapped quickly, allowing for manual removal of spent PCM. This whole process does not rely on external hardware, and can be carried out in mere seconds. Thus, the second approach is taken.

While one PCM module is in operation, the spare is stored in a refrigerator to solidify the PCM. The spare module is expected to be refrigerated for more than 12 hours in-between series of default mode runs. With levitation mode runs less frequent, it is expected that the modules can both be refrigerated before usage, allowing for at least two full runs in a half-day. Considering this, modelling of (and designing for) the cooling process was completely neglected. It is expected that full solidification can occur on these time frames. On the Swissloop testing grounds at Innovationspark Zürich in Dübendorf, a large refrigerator (- 18 °C) can be used.

Heat Transfer Fluid

For the heat transfer between sources and PCM module, a water-based fluid will be used. Water makes for a great heat transfer fluid. Its low viscosity means minimal pumping power usage, whereas the high heat capacity makes for extraordinary heat transfer characteristics.

As an alternative to pumped fluids, heat pipes were considered. While these provide excellent low thermal resistance, they are considerably harder to flexibly integrate than a fluid coolant loop. First, their stiffness requires exact planning and tight tolerances on production, making for additional parts which need to be manufactured. Second, no commercially available heat pipes longer than 600 mm could be found. This presents problems for the application, as 0.6 m is simply too short to link all MOSFETs to the module. It also makes heat pipes unsuitable for large-scale prototypes. While not impossible, building a large evaporation-based heat transfer system was deemed out of scope for this thesis.

3.3 Choice of PCM

Apart from architecture, the choice of PCM is another fundamental design decision for the prototype cooling system. As discussed in Section 2.4, a solid-liquid phase change was identified to be the most promising option for the application at hand.

3.3.1 Temperature of Phase Change

As for the temperature of phase change, the allowed minimum is roughly 37 °C. As discussed in the section defining boundary conditions for the small-scale cooling system (Section 3.1), avoiding impeded functionality at 35 °C is necessary. For the PCMs in use, the phase change does not happen at a discrete temperature. Rather, it occurs over a range of multiple degrees, centered around the temperature of phase change [18]. Thus, for hot summer days, a phase change temperature T_{pc} of at least 40 °C is mandatory. Otherwise, the PCM could start melting simply from natural convection of warm air.

There is, however, a trade-off to elevated T_{pc}. At a given heat flow, all else being equal, the temperature gradient from MOSFET to PCM must be equal. At a higher temperature of phase change, with equal temperature gradient, the electronics are hotter, too. As will be seen later, ensuring sufficient heat transfer with PCMs is a key issue. Thus, from this perspective, reducing T_{pc} is paramount to achieve sufficient heat flow.

3.3.2 Choice of PCM

With paraffin set as the PCM of choice, talks with multiple vendors were initiated. Supply chain issues also made for lackluster availability of some PCMs. For short delivery times and reduced import fees, particular care was given to choosing a supplier within the EU. The paraffin was ordered from Rubitherm Technologies GmbH (Berlin), partly thanks to their good reputation and collaboration with Hochschule Luzern (HSLU). The available Rubitherm product range for paraffin-based PCMs is shown in Table 3.1.

Table 3.1: Rubitherm Paraffin Product Range [26].

	T_{pc}	Δh_{pc}
RT 28 HC	28 °C	220 kJ/kg
RT 31	31 °C	135 kJ/kg
RT 35	35 °C	130 kJ/kg
RT 35 HC	**35 °C**	**210 kJ/kg**
RT 38	38 °C	140 kJ/kg
RT 42	42 °C	135 kJ/kg
RT 44 HC	**44 °C**	**220 kJ/kg**
RT 47	47 °C	130 kJ/kg
RT 50	50 °C	130 kJ/kg
RT 54 HC	54 °C	170 kJ/kg

As mentioned, a low T_{pc} is desirable to improve heat transfer. Meanwhile, T_{pc} needs to be sufficiently high to avoid PCM melting on warm days. To experiment with various T_{pc}, the decision was made to order both RT 35 HC and RT 44 HC. These combine suitable temperature ranges with a high enthalpy of phase change.

At T_{pc} = 35 °C, RT 35 HC is not suited for use on very hot summer days. It is evident that, at temperatures of 35 °C or above, partial melting occurs. However, due to the small temperature gradients of a few degrees, it is unclear if this effect is of relevance in everyday usage. Thus, real-world usage with RT 35 HC at summer ambient temperatures is being conducted. If partial melting significantly affects cooling performance, RT 44 HC is used.

3.4 Simulation of PCM Melting

In order to design the PCM heatspreader, a procedure to model the melting process of the PCM was needed. The simulation of PCM melting processes was conducted in COMSOL 6.0. It allows for customized physics, for example volume forces, non-linear material properties, and for large sweeps using ETH's EULER cluster.

For modelling the PCM, the "heat transfer in solids and fluids" node was coupled with the "laminar flow" node through the "ntif1" multiphysics node. The majority of the model employed here is based on Groulx et al. [27]. The effects of various modelling parameters are explained in detail in [27].

3.4.1 Modelling of Phase Change

Fundamentally, the phase change is modelled by locally varying material properties. The material is modelled as a liquid, but using very high viscosity μ below melting temperature allows for solid-like behaviour. The enthalpy of phase change is represented through a modified heat capacity.

Table 3.2: Modelling Parameters Used in COMSOL.

	Solid		**Liquid**	**T_m**	**35 °C**
rho_s	880 kg/m^3	rho_1	770 kg/m^3	mu_1	0.008 kg/m · s
c_ps	2 kJ/kgK	c_p1	2 kJ/kgK	beta	0.0008 1/K
k_s	0.23 W/mK	k_1	0.18 W/mK	L	210 kJ/kg
				dT	5 K
				A_mush	10^6
				epsilon	10^{-3}

First, a melting temperature T_m is defined over a range dT. Here, these are 35 °C and 5 K respectively. A piecewise linear function $\varphi(T)$ is introduced to express the local liquid fraction of the material as shown in Figure 3.4. Based on this function, the modelled PCM varies its density and thermal conductivity based on the local liquid fraction. The enthalpy of phase change is represented through a modified heat capacity. A gaussian normal distribution based on the width of dT is used. In COMSOL, these material properties can be expressed analytically, meaning no interpolation between discrete values is needed. The modified heat capacity is given by [27]:

$$C_p(T) = c_{ps} + \varphi(T) \cdot (c_{p1} - c_{ps}) + L \cdot e^{-\frac{(T-T_m)^2}{(\Delta T/4)^2}} / \sqrt{\pi(\Delta T/4)^2} \tag{3.1}$$

where ΔT is equivalent to dT, L is the enthalpy of phase change, and c_ps and c_p1 are the specific sensible heat capacities in solid and liquid state. In Equation 3.1, the first two terms represent the linear change in sensible heat capacity, whereas the third term represents the enthalpy of phase change. Table 3.2 shows the material properties used for the model.

The viscosity, on the other hand, is modelled using a Carman-Kozeny function [27]:

$$\mu(T) = \mu_1 + \mu_1 \cdot A_{mush} \frac{(1-\varphi(T))^2}{(\varphi(T))^3 + \varepsilon} \tag{3.2}$$

where A_{mush} influences the high viscosity in solid state, and epsilon (ε) is used to avoid division by 0. Effectively, this function ensures very high viscosity in the solid state and continuously decreasing viscosity with increasing liquid fraction. The viscosity is plotted in Figure 3.4. With $\rho(T)$, $k(T)$, $\mu(T)$ and $C_p(T)$ established, the Navier-Stokes equation and those for diffusive heat transfer are solved in the respective nodes in COMSOL.

To achieve bouancy, a custom volume force was used instead of the "gravity" module. This volume force was formulated as follows:

$$F_B = \rho_1 \beta g (T - T_m) \tag{3.3}$$

where β is the coefficient of thermal expansion for the liquid PCM.

Pressure Point Contraint, Meshing, Transient Solving

Due to a newer version of COMSOL being used, some slight modifications had to be made. In particular, an additional pressure point had to be added to give a boundary condition of pressure.

Like Groulx et al. [27], the problem was simplified to a 2D model, which drastically reduced computational cost. Such a reduction allowed for rapid experimentation with various geometries and optimizing geometries using parameter sweeps to achieve adequate melt fraction at minimal weight. A very fine FE mesh was used with at a maximum 0.5 mm element size.

Liquid/Solid Fraction

To quickly assess the degree of melting in a model, the function $\varphi(T)$ was integrated over the surface area of the 2D model as follows:

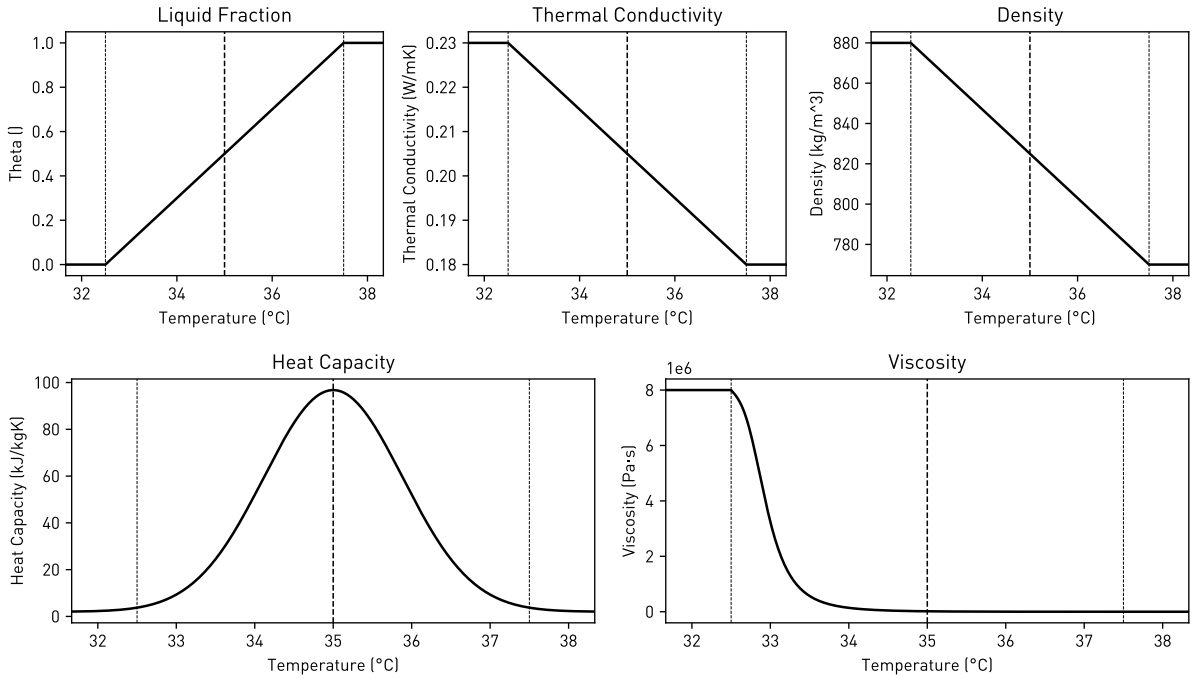

Figure 3.4: Implementation of PCM Material Behaviour for Modelling of Phase Change. The enthalpy of phase change is modelled through an adapted heat capacity. A very high viscosity at temperatures below T_{pc} is used to represent solid behaviour.

$$LF(t) = \frac{1}{A}\int_0^b \int_0^h \varphi(T(x,y,t))dxdy \tag{3.4}$$

where A is the surface of the two-dimensional model, and is used for normalization. Before any melting occurs, LF is 0. Once the PCM is fully melted, LF = 1.0. This variable was used extensively to assess the performance of particular geometries.

3.4.2 Convection

The results obtained by Groulx et al. [27] were successfully reproduced using the aforementioned model including natural convection. However, since solving the Navier-Stokes equations is very computationally intensive compared to solving only heat diffusion, model run times when taking convection into account were significantly higher. Partially, this was also caused by numerical instabilities, which caused simulations to diverge and fail. With the "laminar flow" and "ntif" modules enabled, very tight tolerance criteria and small time-stepping was thus required. These problems were found to be reduced significantly with "laminar flow" and "ntif" disabled. This allowed for more relaxed convergence criteria during time-stepping, and ultimately larger timesteps. For reference, if a simulation taking into account natural convection ran for 3 hours, disabling natural convection would reduce that to roughly 30 seconds.

Furthermore, it was assumed that natural convection in this case exclusively improves heat transfer. Thus, not explicitly simulating this added mode of heat transfer would represent a conservative approach. For these reasons, it was decided to not model natural convection explicitly in COMSOL. Thus, the "laminar flow" module and the multiphysics module "ntif1" which links convection and diffusion, were disabled for all following simulations.

3.5 Modelling Overview

Figure 3.5 provides an overview of the decentralized cooling system. The MOSFET's heat is convectively transferred in the waterblock (R_{wb} and Δp_{wb}). In the centralized module, there is a single water channel

facilitating fluid-heatspreader heat flow (R_c and Δp_c). Both of these were modelled using FloEFD under steady-state conditions. The use of steady-state simulations allowed for extensive experimentation with various geometries and computationally costly optimizations. At the heart of designing the waterblock and module water channel is the trade-off between pressure loss and heat transfer. These are explored in detail in the original thesis [23].

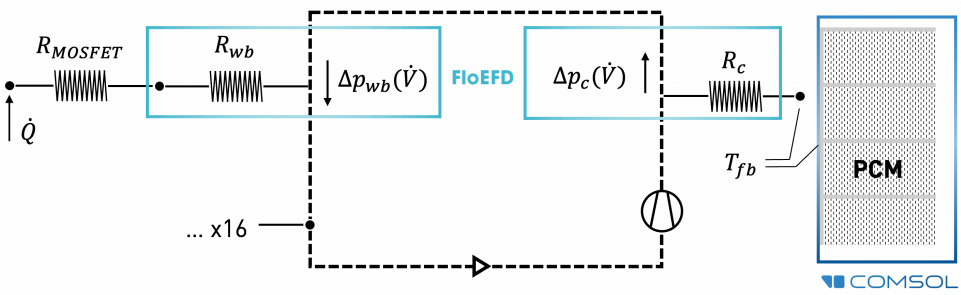

Figure 3.5: Overview of Simulation Strategy. To optimize waterblock and the module's water channel, FloEFD was used. Phase change simulations were conducted in COMSOL in 2D.

The PCM was modelled together with a heatspreader (fin) array in COMSOL. To simplify the interface between the two simulation tools, a fin base temperature T_{fb} of 50 °C was assumed. At 15 °C over the melting temperature of RT 35 HC, good heat transfer is obtainable in the module. A fin base temperature T_{fb} of 50 °C is a conservative working point, since it allows for large temperature differences of roughly 100 °C between the fin base and MOSFET junctions. Fixing T_{fb} early on allowed for simultaneous work in COMSOL and FloEFD, which eased the design process. Towards the end of this chapter, all thermal resistances and pressure losses will be known. A short overview and assessment of system performance will be given.

3.6 Design: PCM Module

The centralized PCM module is fabricated using Selective Laser Sintering (SLS) with an aluminum alloy, AlSi10Mg [28]. While this manufacturing technique is not suited for mass production, single parts can be produced without a cast, mold or similar. Additionally, it enables complex geometries which would not be easily achievable with milling. Lastly, SLS enables the manufacturing of lattice infills, which makes for very strong and light parts. On a lightweight prototype, SLS is thus the perfect manufacturing process for a prototype multi-chamber PCM container.

3.6.1 Structural Design

Structurally, the single largest load occurring on the module originates from internal pressure. This pressure stems from two sources. First, if the cooling system is operating in vacuum, an effective over pressure of 1 bar is experienced in the inside chambers. Second, if the PCM is in its fully melted state, it expands. This expansion causes the air in the PCM chamber to compress, thus causing excess pressure. Since the chambers are sealed to avoid leakage, the module needs to be designed to accommodate the resulting stresses.

Briefly, the idea of incorporating pressure relief valves into the lid was considered. One valve would ensure that the inside pressures over 1 bar would not be exceeded. However, with such a valve, PCM cool-down would cause an under-pressure in the module, even more so after use in near-vacuum. Sub-ambient pressure would cause the fins to be loaded in compression, making for challenging buckling simulations. Thus, another valve would have been added to avoid low pressures. This solution employing two valves was discarded, mostly due to its complexity and the significant weight the valves would introduce.

In addition to internal stresses, the module is designed to accommodate other minor forms of local loads.

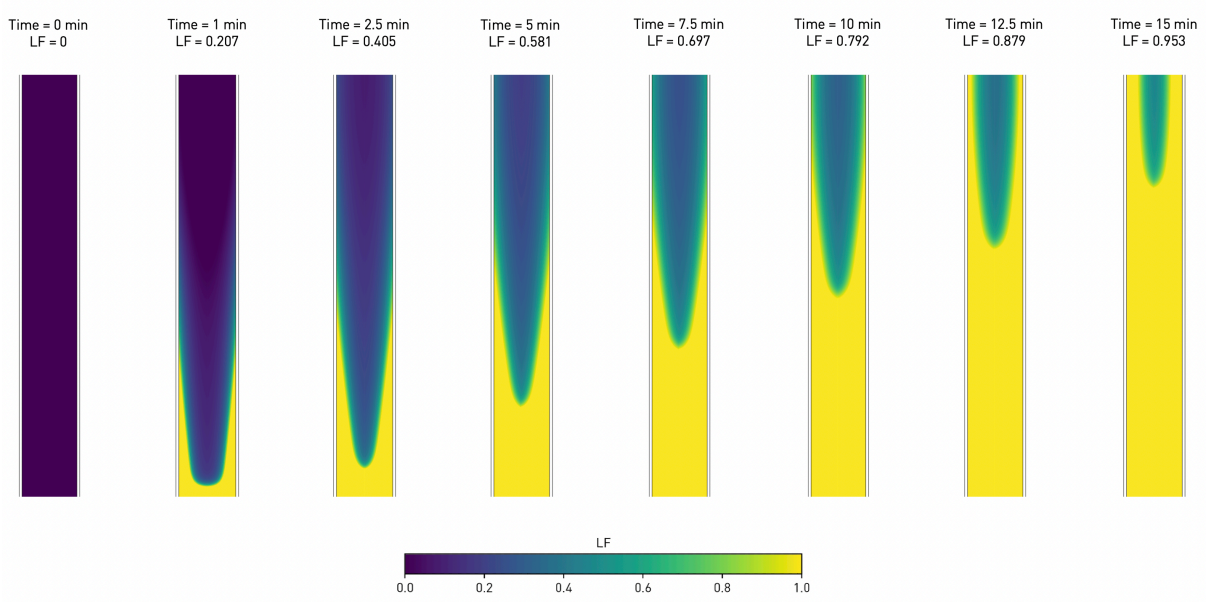

Figure 3.6: Visualization of PCM Melting Process in Optimal Heatspreader Design. Here, the local melt fraction is shown in color. The average melt fraction is denoted at various time steps, reaching 95.3 % at 15 minutes.

Small reinforcements and edge blends are employed around a mounting hardware interface attaching module to vehicle. At the time of writing, the mounting hardware has not been produced.

Airflow and Excess Pressure

Based on the ideal gas law, the pressure p_m inside the module after full melting is given by:

$$\frac{p_m}{p_s} = \frac{V_{air,s}}{V_{air,s} - \Delta V_{pcm}} \tag{3.5}$$

with p_s being the pressure when the PCM is solid, $V_{air,s}$ the overall volume of air within the module if the PCM is solid, and ΔV_{pcm} being the volume change of the PCM upon melting. Here, p_m is set to 1 bar, since the module is sealed when the PCM is cold. Due to seal imperfections, it is assumed that over long periods of time p_s = 1 bar in the module is unavoidable.

To reduce the structural load caused by internal pressure, p_m should be reduced. The module width, length and PCM fill height are given. These have been determined earlier to conform with capacity goals, maximal print dimensions, and heat transfer criteria. Thus, V_{pcm} was considered given. With $V_{air,s}$ as the only tunable design parameter to influence p_m, some steps were taken to increase the internal air volume of the module. As a first step, the air gap between PCM and lid in the chamber was increased to 26 mm. Second, the air volume within the body and lid lattice infills is connected through holes to the PCM chamber. In effect, these holes enable free air flow between the air gap in the PCM chamber and the infill air volumes, significantly increasing $V_{air,s}$. With these steps, p_m is expected to be 1.76 bar.

Structural Design

Despite p_m calculated to be 1.76 bar, the module is designed to tolerate 3 bar. This is for two reasons. First, a catastrophic structural failure would be accompanied by air and PCM rapidly exiting the module. The kinetic energy could cause harm bystanders. Second, the exiting paraffin could damage other vehicle components, rendering custom-made parts useless. Hence, it was designed to allow for more pressure.

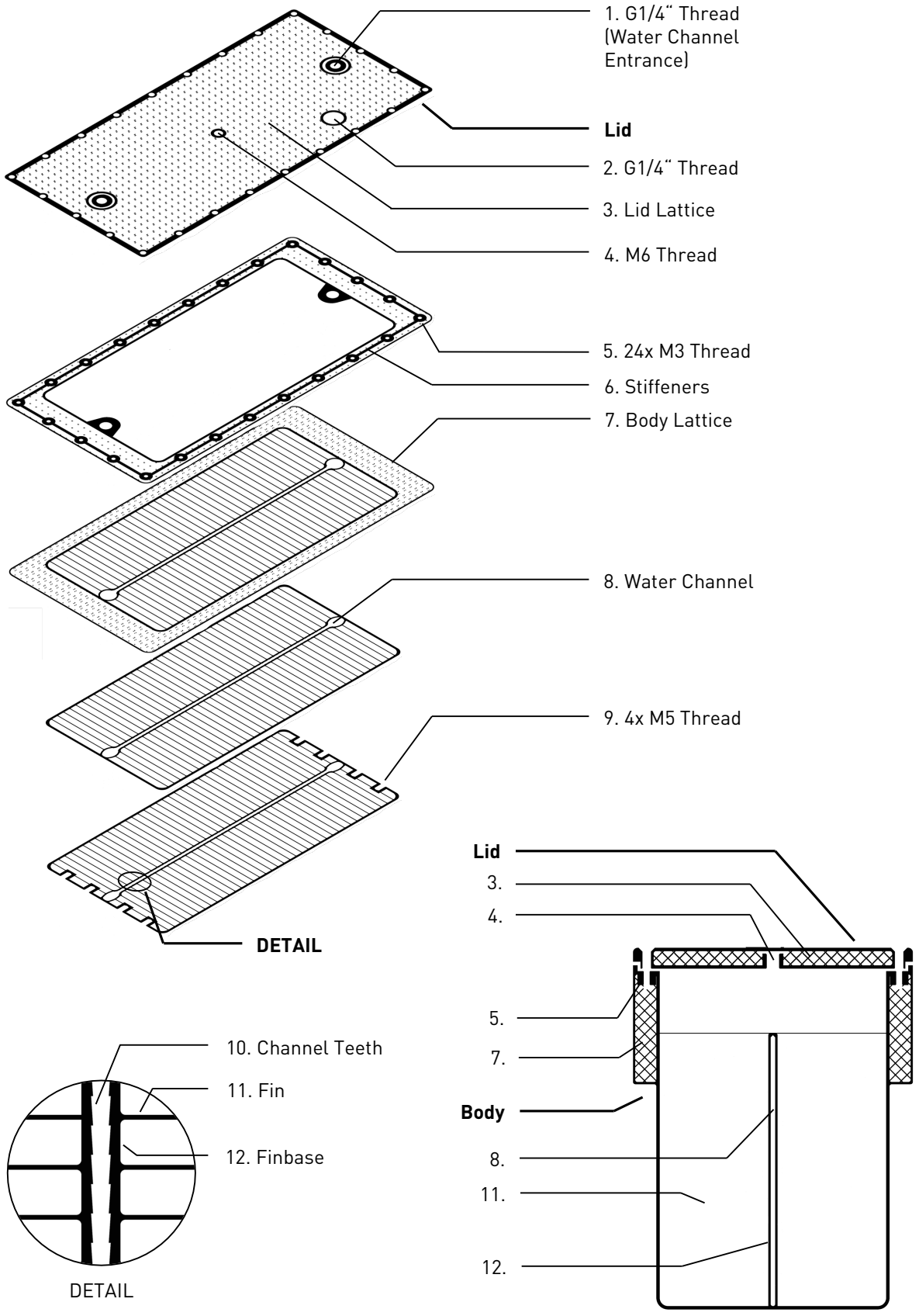

Figure 3.7: Module Cross-Sections. Overview of Key Design Features.

Structurally, the module consists of two main zones. In the lower part of the body, the fins (11. in Figure 3.7) directly transfer the stresses induced by internal pressure between the module walls. Here, the body's outer walls are relatively thin (1.5 mm), since they are directly supported. Meanwhile, in the upper part of the body where no fins are present, the walls are stiffened using a sandwich construction. This is achieved using a lattice core. Between the section with stiffened walls and that supported by fins, there is a 10 mm overlap to reduce stress concentrations. The core (body lattice, 7. in Figure 3.7) thickness is 10 mm along the long edge and 20 mm at the short edge of the body.

Like the body's upper part, the lid is constructed using 1.5 mm face sheets and a 6 mm core. At below 400 g, it is significantly lighter than an equivalently strong CNC milled part. The lid lattice core (3. in Figure 3.7) is reinforced by a solid lip around the lid's edges. This solid frame takes up screw compression and stiffens the gasket interface. Similarly, the body is equipped with stiffeners (6. in Figure 3.7) . At a height of 6 mm, these significantly increase the rigidity of the body's gasket surface. This, in turn, decreases the likelihood of leaks upon loading with higher pressures.

The lattice structure chosen for the body and lid is "dode" with a unit length of 5 mm, and approximately 15 % volumetric infill. It was chosen since the manufacturer (Feramic AG, Stallikon) has extensive experience with this lattice type. On the lid, the air entrance hole as shown under 4. in Figure 3.7 contains an M6 thread. On this thread, a GORE PolyVent XS plug [29] is mounted. It is fitted with a membrane, allowing air to freely pass while blocking the flow of paraffin. This avoids contamination of the lid core with PCM during rapid accelerations and decelerations when levitating.

FEM Structural Analysis

Finite Element Method (FEM) structural analysis was performed on both lid and body using Siemens NX Nastran. The structural modelling is described in detail in the original thesis [23]. The module and lid were simulated with 3 bar of internal pressure. A safety factor of 3.3 could be reached.

3.6.2 Module Overview

Figures 3.8 and 3.9 show the finished module shortly before PCM fill-in. The lattice 20 mm at the ends to make for an integrated handle.

Figure 3.8: Finished Module Body without Lid, Gasket and PCM.

Figure 3.9: Finished Module with Lid, Pressure Sensor, and Quick Connectors.

3.7 Design: Waterblocks and Integration

In the original thesis [23], the optimization and final design of the waterblocks is described in great detail. These are mounted to the MOSFETs of the power electronics and ensure heat transfer from MOSFET into the cooling water.

Additionally, the thesis covers other aspects of the finished cooling system design, such as the choice of pump, the tubing used, fluid couplings, and sensors for temperature and internal pressure measurements.

As for the heat transfer fluid, all simulations and calculations were carried out with pure water. For the finished system, a glycol-water mixture with freezing point of - 18 °C was used. Such low temperatures allow for faster cool-down and solidification of the PCM in a freezer. Additionally, a bactericide and anti-corrosion agent were added.

Both a pressure sensor and inlet / outlet thermistors can be used to calculate the overall liquid fraction of the PCM. With the thermistors, an energy balance of the in- and outflowing water can be integrated over time to find the energy absorbed by the module. Additionally, the pressure sensor can measure the thermal expansion the PCM has undergone by measuring the internal pressure. The overall melt fraction can then be computed via the measured expansion. This technique depends on a perfect seal of the modules air/PCM chamber.

3.8 Safety

Some safety aspects of the system are treated in the 2023 Swissloop TSD in detail. Treated here are two points unique to PCM cooling systems.

First, paraffin is flammable. However, the flash point for RT 35 HC is 177 °C [18]. Reaching such temperatures is only regarded as a possibility if other vehicle components, for example the Li-Ion batteries,

experience thermal runaway. In a case associated with electrical failure, the paraffin could potentially be ignited since the aluminium module is electrically conductive. However, the internal volume of air is restricted, meaning only a small fraction of the paraffin could burn off. Whether or not this limited burn-off could lead to internal pressures and temperatures which damage the module and lead to a kinetic risk has not been checked.

Second, excessive internal pressure more generally can cause a kinetic risk. While there are few situations that could cause internal pressures over 3 bar, the built-in pressure sensor can be used for monitoring.

3.9 Overview

Table 3.3 shows the overall system mass. The ratio of PCM to metal mass is roughly 50 %. On the body, the weight is distributed roughly equally between heat transfer devices (fins, water channels) and structural features (walls, lattice and air pockets). Figure 3.10 shows the finalized cooling system on the 2022/2023 Swissloop vehicle.

Table 3.3: System Mass Overview.

Module	1853 g
PCM	1727 g
Water	450 g
Tubing	230 g
Waterblocks	1720 g
Pump	235 g
Quick Connectors	100 g
Sensors	300 g
Total	**6615 g**

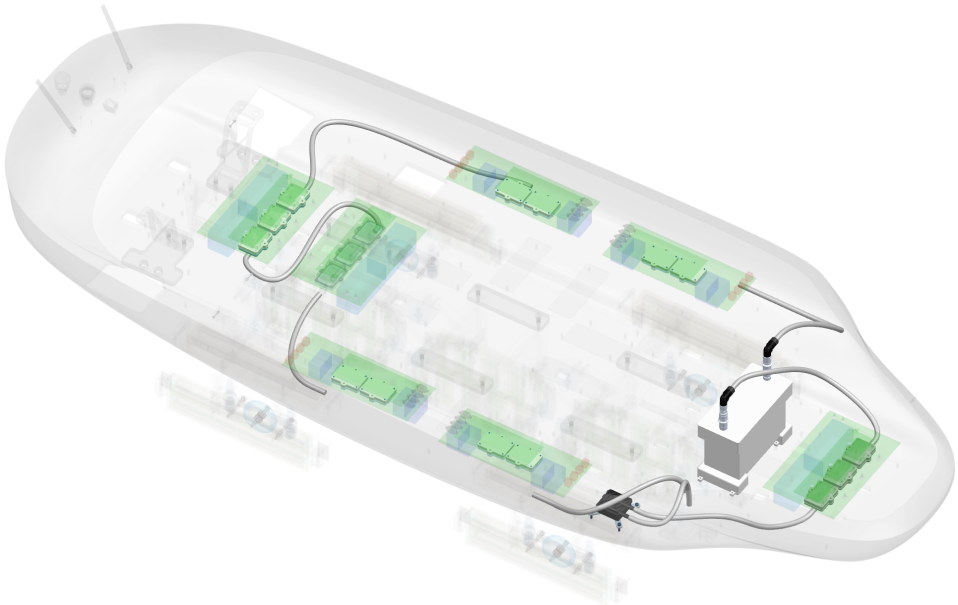

Figure 3.10: System Overview in CAD (Siemens NX).

Manufacturing and Testing

4.1 Manufacturing

As for the manufacturing and initial comissioning, the thesis [23] goes into extensive detail. Described here are a few points of note.

4.1.1 PCM-Fill-In

Filling in the paraffin was done by melting it and simply pouring it into the module. Heating of the paraffin was achieved using an industrial oven at 60 °C and took roughly 8 hours for 12 kg of paraffin in a plastic container. The module was specifically designed to enable all fins and paraffin cavities to be visible and easily accessible. After fill-in, the module was placed in the oven at 60 °C for roughly one hour to eliminate air pockets.

4.1.2 Commissioning

The module was comissioned in late January. However, real conclusions on overall system performance will only be drawn once the 2022/23 season comes to a conclusion.

4.1.3 Vacuum Testing

The whole system is built for operation in vacuum, both from a thermal and structural standpoint. However, no adequate testing facilities were found, so that these tests unfortunately had to be left out.

Design for Full-Scale

To reiterate, the numbers assumed here are not necessarily in agreement with contemporary assumptions on full-scale power consumption. No system-wide analysis of the full-scale cooling requirements posed by propulsion, levitation and other subsystems has been conducted to keep the scope of this thesis reasonable.

Rather, focus was put on designing a PCM cooling system and presenting specific learnings applicable to full-scale implementation. Here, mass and performance trends of full-scale PCM systems are drawn up based on 4 kW and 8 kW heat generation over 15 minutes up to one hour.

5.1 System Architecture

As for the prototype system described above, it currently appears that a centralized architecture is favourable in a full-scale scenario. Many of the same advantages apply. The primary of these is fast replacement of liquid PCM. Figure 5.1 shows a concept for automated quick-swapping between vehicle runs. A robotic arm can replace a combined battery and PCM module in a matter of seconds, replenishing electrical energy and thermal capacity. To add to that, a decentralized architecture allows for cooling almost all component types (levitation systems, motor, electronics) thanks to its flexibility. This advantage has been explained in detail in Section 3.2.2.

If longer timeframes for the retrieval of heat can be tolerated, retrieving heat with a coolant loop can provide a good alternative. If a coolant loop is used for flushing, a decentralized architecture can be used. The advantageous heat transfer characteristics can translate to potential weight savings. However,

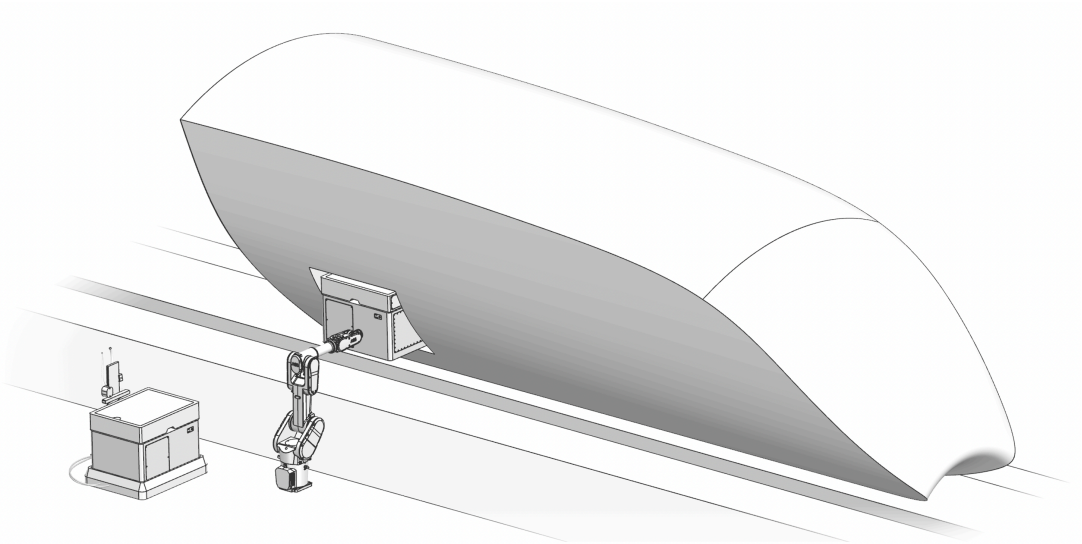

Figure 5.1: Robotic Quick-Swapping Concept for PCM Module. After exchanging the module, it can be cooled over reasonable time frames. The PCM module can be integrated into a single module with a battery for energy storage.

cooling of different component types in various shapes requires significantly more design and simulation work.

5.2 Choice of PCM

The broad range of phase change mechanisms has been explored in Section 2.4. As discussed, salt hydrates and paraffin are considered the most feasible solutions for full-scale applications. Of these, paraffin was chosen for the small-scale cooling module built here. Due to corrosion, cyclical stability and manufacturer reputation as major downsides salt hydrates were excluded. As such, the decision to deploy paraffin was taken primarily due to practical constraints.

As alluded to in Section 2.4 and shown in Figure 2.5, salt hydrates come with potential weight savings due to their high density and thermal conductivity. The associated decrease in volume and heat transfer requirements promises to reduce enclosure and heatspreader mass. To explore this advantage in detail, large sweeps were conducted in COMSOL to compare three PCM materials.

5.2.1 Simulation

Paraffin, hydrated salt and a paraffin with additives were simulated for a full-scale module. Table 5.1 shows the material values of these. The overall system mass of paraffin with additives compared to hydrated salt was of particular interest. The material data is based on commercially available PCMs [16, 18, 26] and the findings from Section 2.4.4.

Table 5.1: Material Data for Full-Scale PCM Simulations

	Paraffin	**Hydrated Salt**	**Paraffin + 4% CF**
h_{pc} (kJ/kg)	210	180	200
k_s (W/mK)	0.2	0.5	1.2
ρ_s (kg/m^3)	880	1570	920
$c_{p,s}$ (kJ/kgK)	2	2	2

Simulations were carried out for four power scenarios. A 440 W, 15 minute load was carried out representing the small-scale module shown above. A 4 kW, 15 minute was simulated to represent a low-

capacity, high heat transfer scenario. Finally, full-scale scenarios of 4 kW and 8 kW respectively over 1 hour were simulated. Two parameters, the fin width and amount of fins could be varied. With this variation, the module mass varied. The quality of heat transfer was assessed by measuring the liquid fraction.

Model Setup

The model employed here is very similar to that used earlier for the optimization of the small-scale system. The setup is described in detail in the original thesis [23].

Results

Figure 5.2 shows the results of the simulations. The melt fraction (or liquid fraction LF) at the final time step is shown for each parameter combination in color. Mass iso-lines are also shown. For each material and power scenario, the optimal solution was identified. A necessary condition of achieving 100 % LF was implemented for viable solutions. Of these, the one with minimal overall mass was chosen. The system mass and PCM mass fraction of these optimal solutions are displayed in each plot.

Multiple insights can be formulated from these results. First, system mass obtained for the 440 W, 15 minute scenario is significantly higher than what was achieved in the real world. Whereas the modelled paraffin module weighs at least 8.5 kg in these sweeps, the module shown earlier weighs only 3.85 kg, corresponding to more than a 50 % weight optimization. The large difference can be attributed to an assumption of 5 mm outer wall thickness in the simulation here, which is not valid for small modules since the internal pressure can be handled using thinner walls at lower volumes. Therefore, the mass and PCM fraction of a carefully designed thermal management system could be reduced greatly compared to the values obtained here.

Second, the use of additives pays off. In all cases, the simulated full-scale modules which employ additives in paraffin outperform pure paraffin. No further investigation has been conducted, but this is seen as a strong indication that employing graphite or carbon fiber additives comes with significant mass savings depending on the power scenario.

Third, hydrated salt consistently outperforms the other two materials. Despite lower thermal conductivity than paraffin with additives, the mass fraction when using hydrated salt is the highest for all cases. Due to their high density, salt hydrates shorten the effective thermal path through the PCM and thus improve heat transfer. Additionally, the high density gives salt hydrates an advantage in terms of volume occupied by the module. As alluded to earlier, this can be a high priority in full-scale systems, where a passenger cabin is associated with disproportionate space consumption.

Lastly, for short, high-power scenarios the PCM mass fraction is low. Since the heatspreader has to be enlargened, it contributed more mass to the overall system. The masses of the optimal solutions from Figure 5.2 are shown in Figure 5.3. All of these solutions achieve rather low PCM mass fractions, with a maximum of 67 % PCM for hydrated salt at 8 kW over 60 min. However, the PCM is still responsible for the majority of available thermal capacity. More details can be found in the original thesis [23].

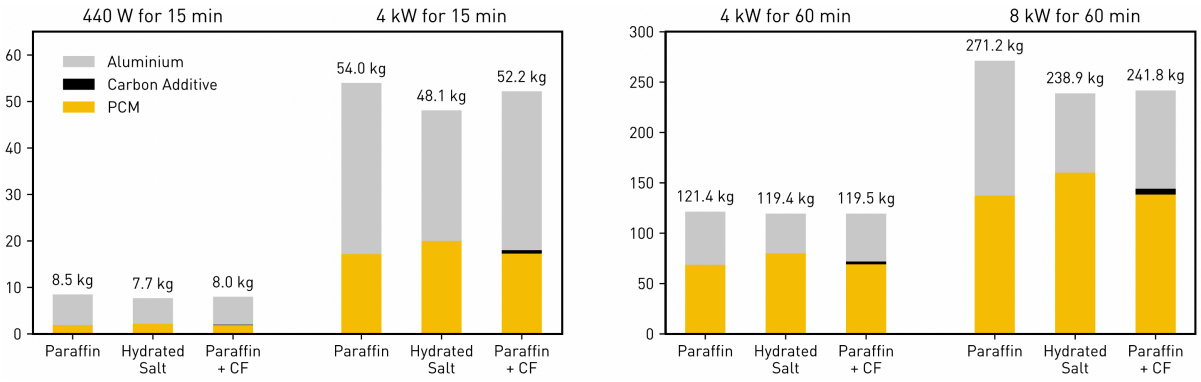

Figure 5.3: Mass Fractions of PCM Types in Full-Scale Scenario.

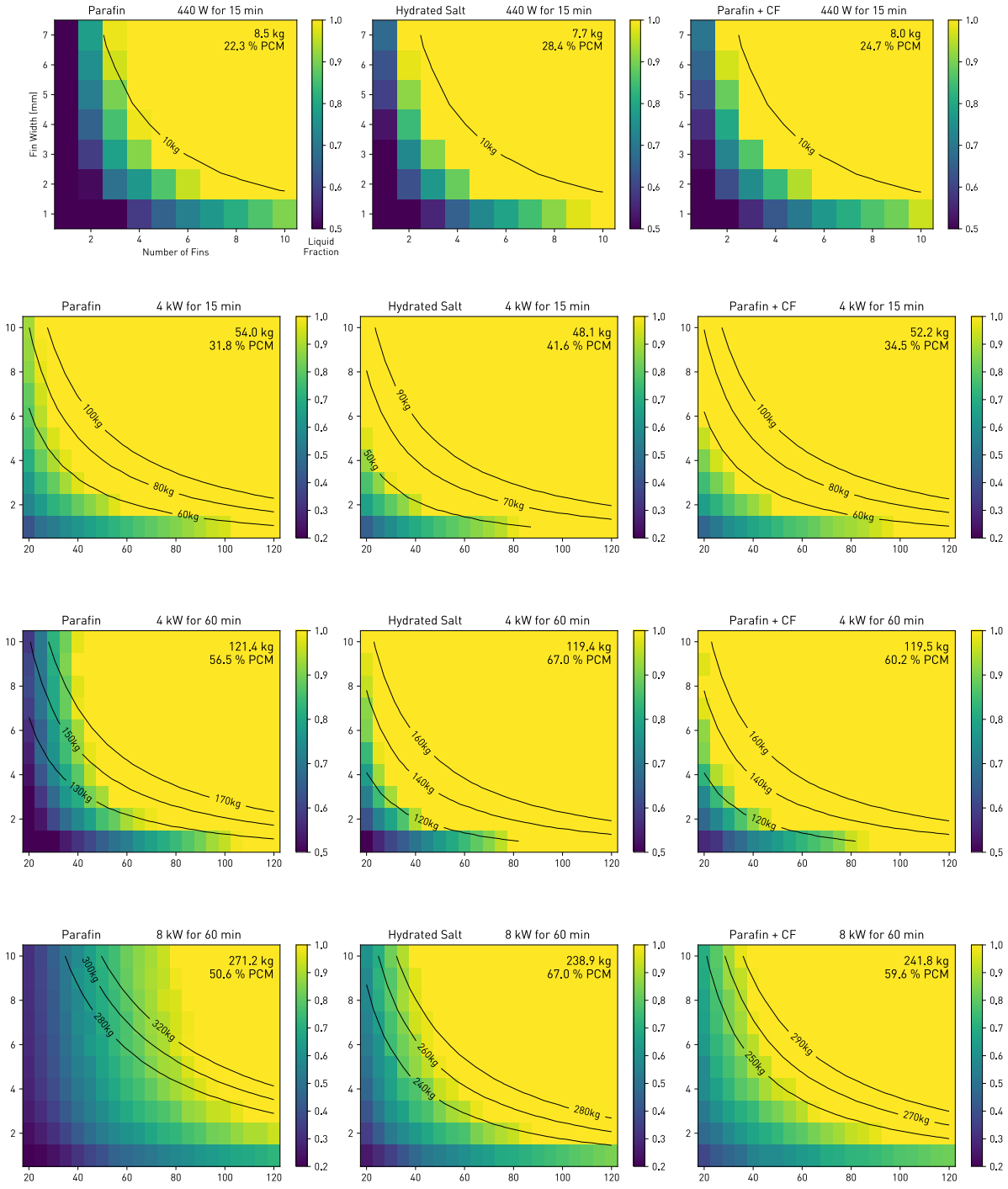

Figure 5.2: Melt Fraction and Overall Module Mass of PCM Types in Full-Scale Scenario. Each data point represents an individually simulated parameter combination.

Conclusion

In the thesis, approaches to thermal management in Hyperloop vehicles were discussed. Then, a fully functional prototype of a latent heat storage device was designed, manufactured and commissioned.

Full-Scale Thermal Management Concepts

Various means of thermal management in Hyperloop vehicles were examined to asses their viability. Some concepts can be excluded with a high degree of confidence. Convection at low pressures (10 mbar) has been shown to not provide adequate dissipative performance. Dedicated sensible heat storage, in particular if made from metals, has proved to be significantly heavier than a PCM alternative. Sensible heat storage in a component with combined structural/thermal usage can also be ruled out due to heat leakage and difficult heat retrieval.

Using a liquid-gaseous phase change was not pursued further. In terms of mass-specific performance, this approach is very promising. However, the retrieval of vapor from Hyperloop tubes has not been assessed and might pose a great challenge.

Some thermal concepts have been identified as potentially viable, although with some drawbacks. One of these is convection, which can be sufficient at higher tube pressures of around 100 mbar. However, adequate airflow over a large and heavy fin array must be ensured. The skin drag such a radiator would introduce is seen as a large downside of this method. It needs to be examined in detail. Radiation, under the tested circumstances, can also provide sufficient dissipation. It can be achieved by leveraging the large surface area of the outer fairing, or by heating a well-isolated probe. For the former, adequate isolation of the fairing to prevent heat leakage is needed. Additionally, ensuring homogeneous fairing temperatures poses a significant challenge, since the fairing's in-plane thermal conductivity needs to be good.

Finally, latent heat storage has been identified as a promising option for full-scale thermal management in Hyperloop applications. As shown, paraffin or salt hydrate PCM units can be built at moderate weight for one hour runs in the single-digit kW range. These units can be scaled easily depending on the power profile. Solid-solid phase change materials were ruled out due to their low specific enthalpy of phase change.

Phase Change Cooling System

During the design phase of the prototype cooling system, major design considerations such as the choice of components to cool, the architecture, choice of PCM, melting temperature and whether to use additives have been weighed.

Various advantages and drawbacks of centralized and decentralized architecture were discussed. Ultimately, the architectural design of a PCM cooling system is highly dependent on the vehicle type and operational scenario. Here, the choice was made to pursue a centralized approach. By doing so, the module can be quick-swapped, and various component types can easily be integrated into the coolant loop without requiring an adapted PCM module design. Here, water serves as a heat transfer medium, and acts as a buffer during short bursts of heat output.

A melting temperature of roughly 35 °C - 45 °C was determined to be suitable for use on hot summer days. A paraffin-based PCM was chosen due to its large enthalpy of phase change, the abundance of literature on the material, cyclical stability, availability, manufacturer reputation and non-corrosiveness. A common alternative to paraffin are salt hydrates, which perform worse in these regards and were thus not pursued further. However, the high thermal conductivity and high density of salt hydrates can enhance heat transfer greatly. This leads to a decrease in heatspreader mass. Additionally, the low volume makes for more compact systems.

The use of additives to enhance thermal conductivity was omitted due to time constraints. However, as has been shown in Section 5.2.1, additives can increase thermal conductivity in the PCM drastically and thus reduce heatspreader mass. There is extensive literature on the subject, which can be used in future work.

For the heatspreader, a central channel approach with thin fins was used here. While the performance of this approach has been found to be adequate for the application at hand, other geometries could potentially be investigated in the future.

Two major challenges which were not expected at the outset were encountered while designing the prototype PCM module. First, thermal expansion poses a large problem for closed PCM containers. Structural reinforcement and enlargened air pockets to buffer the effect are indispensable. Second, PCMs can affect the choice of materials in the containers used. For example, a gasket material (NBR) which can tolerate paraffin had to be chosen.

Bibliography

[1] Manuel Häusler. *Cooling Concept for Hyperloop Pod Prototypes*. Tech. rep. Hochschule Luzern, 2019.

[2] Denis Tudor and Mario Paolone. "Operational-driven optimal-design of a hyperloop system". In: *Transportation Engineering* 5 (Sept. 2021), p. 100079. ISSN: 2666-691X. DOI: 10.1016/J.TRENG.2021.100079.

[3] Nishanth Dongari, Ashutosh Sharma IITK, and F Durst. "Pressure-driven diffusive gas flows in micro-channels: From the Knudsen to the continuum regimes". In: *Microfluidics and Nanofluidics* 6 (Jan. 2009), pp. 679–692. DOI: 10.1007/s10404-008-0344-y.

[4] VDI Gesellschaft Verfahrenstechnik und Chemieingenieurwesen. *VDI-Wärmeatlas, 11. Auflage*. Tech. rep. 2013.

[5] Paul Allen Tipler and Gene Mosca. *Physik für Wissenschaftler und Ingenieure*. 7th ed. Berlin; Heidelberg: Springer Spektrum, 2015, pp. 556–558.

[6] Laboratory of Thermodynamics in Emerging Technologies. *Formelsammlung Thermodynamik II – Teil II*. Zurich: ETH Zurich, 2021.

[7] H. Wu et al. "Characterization of thermal cross-talk in a MEMS-based thermopile detector array". In: *Journal of Micromechanics and Microengineering* 19.7 (2009). ISSN: 09601317. DOI: 10.1088/0960-1317/19/7/074022.

[8] Federico Lluesma et al. "Evacuated-Tube, High-Speed, Autonomous Maglev (Hyperloop) Transport System for Long-Distance Travel: An overview". In: *IEEE Electrification Magazine* 9.4 (Dec. 2021), pp. 67–73. ISSN: 23255889. DOI: 10.1109/MELE.2021.3115543.

[9] Reza Shokrollah Abhari and Aldo Steinfeld. *List of Equations for Thermodynamics III*. PREC, 2021.

[10] Moran and Shapiro. *Fundamentals of Engineering Thermodynamics: Appendix*. 3rd ed. New York: J. Wiley & Sons, 1995. ISBN: 978-0471076810.

[11] National Institute of Standards and Technology. *NIST Chemistry WebBook, SRD 69*. 2021. URL: https://webbook.nist.gov/cgi/cbook.cgi?ID=C75150&Mask=4.

[12] National Institute of Standards and Technology. *NIST Chemistry WebBook, SRD 69*. 2021. URL: https://webbook.nist.gov/cgi/inchi?ID=C79209&Units=SI&Mask=4#Thermo-Phase.

[13] Ali Fallahi et al. *Review on solid-solid phase change materials for thermal energy storage: Molecular structure and thermal properties*. 2017. DOI: 10.1016/j.applthermaleng.2017.08.161.

[14] PCM Products Ltd. *PlusICE Solid-Solid (X) Range*. 2018. URL: https://www.pcmproducts.net/files/X%20range-2018.pdf.

[15] Lingai Luo and Nolwenn Le Pierrès. "Innovative Systems for Storage of Thermal Solar Energy in Buildings". In: *Solar Energy Storage* (Jan. 2015), pp. 27–62. DOI: 10.1016/B978-0-12-409540-3.00003-7.

[16] Rubitherm Technologies GmbH. *Technical Datasheet SP 31*. 2022. URL: https://www.rubitherm.eu/media/products/datasheets/Techdata_-SP31_DE_12072022.PDF.

[17] Rubitherm Technologies GmbH. *Technical Datasheet SP 70*. 2020. URL: https://www.rubitherm.eu/media/products/datasheets/Techdata_-SP70_DE_24112020.PDF.

[18] Rubitherm Technologies GmbH. *Technical Datasheet RT35HC*. 2020. URL: https://www.rubitherm.eu/media/products/datasheets/Techdata_-RT35HC_EN_09102020.PDF.

[19] F. Frusteri et al. "Thermal conductivity measurement of a PCM based storage system containing carbon fibers". In: *Applied Thermal Engineering* 25.11-12 (Aug. 2005), pp. 1623–1633. ISSN: 13594311. DOI: 10.1016/j.applthermaleng.2004.10.007.

[20] Jun Fukai et al. *Thermal conductivity enhancement of energy storage media using carbon Fibers*. Tech. rep. URL: www.elsevier.com/locate/enconman.

[21] Ali Karaipekli, Ahmet Sari, and Kamil Kaygusuz. "Thermal conductivity improvement of stearic acid using expanded graphite and carbon fiber for energy storage applications". In: *Renewable Energy* 32.13 (Oct. 2007), pp. 2201–2210. ISSN: 09601481. DOI: 10.1016/j.renene.2006.11.011.

[22] V. Shatikian, G. Ziskind, and R. Letan. "Numerical investigation of a PCM-based heat sink with internal fins". In: *International Journal of Heat and Mass Transfer* 48.17 (Aug. 2005), pp. 3689–3706. ISSN: 00179310. DOI: 10.1016/j.ijheatmasstransfer.2004.10.042. URL: shatikian05.

[23] Tim Aebersold. *Design, Simulation and Manufacturing of a Phase Change Cooling Module for Low-Pressure Applications*. Tech. rep. Zurich: ETH Zurich, Feb. 2023. URL: https://polybox.ethz.ch/index.php/s/XtAWKGybhvWzjaT.

[24] Luvata (Mitsubishi Materials Corp.) *Copper Hollow Conductors*. Tech. rep. 2018. URL: https://cdn.luvata.com/docs/default-source/products/hollow-conductors/copper-hollow-conductors_eng.pdf?sfvrsn=d5ed800a_25.

[25] Carl Brander and Lukas von Briel. "Swissloop Focus Project 21/22 Final Report". In: (2022).

[26] Rubitherm Technologies GmbH. *Rubitherm Webpage PCM RT-Serie*. 2023. URL: https://www.rubitherm.eu/produktkategorie/organische-pcm-rt.

[27] Ali C Kheirabadi and Dominic Groulx. *SIMULATING PHASE CHANGE HEAT TRANSFER USING COMSOL AND FLUENT: EFFECT OF THE MUSHY-ZONE CONSTANT*. Tech. rep. 6. 2015, pp. 427–440.

[28] GE Additive. *Datasheet AlSi10Mg M2 Multilaser*.

[29] W. L. Gore & Associates GmbH. *GORE® Protective Vents Catalogue*. 2021. URL: https://www.distrelec.ch/Web/Downloads/_t/ds/WLGore_ScrewIn_Vents_eng_tds.pdf.